Since January 2020 Elsevier has created a COVID-19 resource centre with free information in English and Mandarin on the novel coronavirus COVID-19. The COVID-19 resource centre is hosted on Elsevier Connect, the company's public news and information website.

European Journal of Medicinal Chemistry 215 (2021) 113242

Contents lists available at ScienceDirect

European Journal of Medicinal Chemistry

journal homepage: http://www.elsevier.com/locate/ejmech

Discovery and structural optimization of 3-*O*-β-chacotriosyl oleanane-type triterpenoids as potent entry inhibitors of SARS-CoV-2 virus infections

Hui Li [a, 1], Chen Cheng [b, 1], Sumei Li [c, 1], Yan Wu [d], Zhihao Liu [a], Mingjian Liu [a], Jianxin Chen [e], Qiuyu Zhong [a], Xuesha Zhang [a], Shuwen Liu [b, f, **], Gaopeng Song [a, *]

[a] *Key Laboratory for Biobased Materials and Energy of Ministry of Education, College of Materials and Energy, South China Agricultural University, Guangzhou, 510642, China*
[b] *Guangdong Provincial Key Laboratory of New Drug Screening, School of Pharmaceutical Sciences, Southern Medical University, Guangzhou, 510515, China*
[c] *Department of Human Anatomy, School of Medicine, Jinan University, Guangzhou, 510632, China*
[d] *State Key Laboratory of Virology, Wuhan Institute of Virology, Center for Biosafet Mega-Science, Chinese Academy of Sciences, Wuhan, 430071, China*
[e] *Guangdong Provincial Key Laboratory of Veterinary Pharmaceutics Development and Safety Evaluation, College of Veterinary Medicine, South China Agricultural University, Guangzhou, 510642, China*
[f] *State Key Laboratory of Organ Failure Research, Guangdong Provincial Institute of Nephrology, Southern Medical University, Guangzhou, 510515, China*

ARTICLE INFO

Article history:
Received 7 December 2020
Received in revised form
18 January 2021
Accepted 25 January 2021
Available online 8 February 2021

Keywords:
3-*O*-β-chacotriosyl saponins
SARS-CoV-2 entry inhibitors
Structure-activity relationships

ABSTRACT

Currently, SARS-CoV-2 virus is an emerging pathogen that has posed a serious threat to public health worldwide. However, no agents have been approved to treat SARS-CoV-2 infections to date, underscoring the great need for effective and practical therapies for SARS-CoV-2 outbreaks. We reported that a focused screen of OA saponins identified 3-*O*-β-chacotriosyl OA benzyl ester **2** as a novel small molecule inhibitor of SARS-CoV-2 virus entry, via binding to SARS-CoV-2 glycoprotein (S). We performed structure-activity relationship profiling of **2** and discovered C-17-COOH of OA was an important modification site that improved both inhibitor potency toward SARS-CoV-2 and selectivity index. Then optimization from hit to lead resulted in a potent fusion inhibitor **12f** displaying strong inhibition against infectious SARS-CoV-2 with an IC_{50} value of 0.97 μM *in vitro*. Mechanism studies confirmed that inhibition of SARS-CoV-2 viral entry of **12f** was mediated by the direct interaction with SARS-CoV-2 S2 subunit to block membrane fusion. These 3-*O*-β-chacotriosyl OA amide saponins are suitable for further optimization as SARS-CoV-2 entry inhibitors with the potential to be developed as therapeutic agents for the treatment of SARS-CoV-2 virus infections.

1. Introduction

As with other well-known coronaviruses (CoVs) such as severe acute respiratory syndrome CoV (SARS-CoV) and Middle East respiratory syndrome CoV (MERS-CoV), severe acute respiratory syndrome coronavirus 2 (SARS-CoV-2) is a new enveloped positive-stranded RNA virus [1–4]. SARS-CoV-2 is able to cause high pathogenic and apathogenic human infections because of the possibility of an aerosol mode of transmission, the high fatality rate, as well as the unpredictable nature of the outbreaks, posing a serious threaten to public health and the global economy [5–7]. The outbreak of novel coronavirus disease 2019 (COVID-19) caused by SARS-CoV-2 has resulted in over 61.8 million infections and over 1.4 million deaths worldwide [8], which underscores the need for drug discovery and development efforts to obtain available treatments. There are no clinically effective vaccines for the prevention of COVID-19 infections though several SARS-CoV-2-specific vaccines have entered a Phase III trial [9,10]. In addition, only a few compounds such as lopinavir/ritonavir, chloroquine, hydroxychloroquine and remdesivir have advanced to clinical trials, but they displayed the limited curative effect and toxic side effects for

* Corresponding author.
** Corresponding author. Guangdong Provincial Key Laboratory of New Drug Screening, School of Pharmaceutical Sciences, Southern Medical University, Guangzhou, 510515, China.
E-mail addresses: liusw@smu.edu.cn (S. Liu), songgp1021@scau.edu.cn (G. Song).
[1] These authors contributed equally to this work.

https://doi.org/10.1016/j.ejmech.2021.113242
0223-5234/

the treatment of COVID-19 patients [11,12]. Thus, there is still an urgent need to develop specific anti-SARS-CoV-2 agents offering efficacy and safety, which can be used alone or in combination with vaccines in future infections.

The surface structural spike glycoprotein (S) of SARS-CoV-2 virus plays a vital role in mediating virus entry into host cell that is the first step in the infection process [13,14]. Structurally, the SARS-CoV-2 S glycoprotein exists as a homotrimer with multiple glycosylation sites and consists of two subunits, an N-terminal S1 subunit and a C-terminal S2 subunit. After SARS-CoV-2 S1 subunit recognizes the cellular ACE2 receptor via receptor-binding domain (RBD), S2 subunit will change its conformation to regulate S-mediated viral/cell membrane fusion [15,16]. Blocking S glycoprotein can prevent SARS-CoV-2 entry into the cell and downstream replication processes, which provides important clues for overcoming SARS-CoV-2.

The SARS-CoV-2 S protein is of particular interest for antiviral development due to its ability in bonding to the human ACE2 receptor, generating membrane fusion events that make possible for the virus to penetrate host human cells [17,18]. Recently, certain antibodies have been found to exhibit potency toward SARS-CoV-2 *in vitro*, which directly bond to the S1 subunit to inhibit SARS-CoV-2 [19–21]. As is the case for effective SARS-CoV-2-S antibodies, great efforts have been made to identify specific small-molecule entry inhibitors of SARS-CoV-2 on the basis of multiple high-throughput virtual screens of various small-molecule libraries. To our best knowledge, only limited examples of inhibitors that bind directly to the SARS-CoV-2 S protein in enzymatic assays have been reported up to now, including glycyrrhizic acid (**GL**, Fig. 1A) that are suggested to block the interaction between RBD domain of the SARS-CoV-2 S1 subunit and ACE2 [22], and Salvianolic acid C (**Sal-C**, Fig. 1A) that was found to block the formation of six-helix bundle (6-HB) core of S2 protein to inhibit membrane fusion [23]. Despite the fact that more data are needed to prove their antiviral efficacy *in vitro* or *in vivo*, the discovery of these known antibodies and small-molecule entry inhibitors highlights SARS-CoV-2 S protein as a promising target for the development of novel anti-SARS-CoV-2 therapeutics.

Oleanolic acid (**OA**), is the most well-known oleanane-type pentacyclic triterpene, of which analogs/derivatives have been confirmed in many studies to exert a variety of antiviral activities against human immunodeficiency virus (HIV), influenza A virus (IAV), Ebola virus (EBOV) and hepatitis C virus (HCV) [24–27]. Interestingly, certain OA derivatives are found to display potential inhibition toward IAV entry as does **GL** [28,29]. Further investigations suggested that these triterpenoids are able to directly bind to multiple viral glycoproteins including GP41 of HIV, hemagglutinin (HA) of influenza, and GP of EBOV, thereby blocking virus-host fusion to disrupt viral entry into the host cells [27]. In particular, CoVs belong to "Type I" fusion proteins as do other well-known enveloped viruses such as HIV, IAV, and EBOV. Evidence has revealed that these enveloped viruses might have the similar entry mechanism in spite of different cell receptors and diverse glycoproteins [30,31]. Based on these results, it can be assumed that OA derivatives is a potential scaffold for the discovery of potential entry inhibitors of SARS-CoV-2 virus.

From the last decade, our research group has been involved in the discovery and development of novel IAV entry inhibitors structurally relate to OA trisaccharide saponins [27,28,32], which are capable of blocking HA2-mediated membrane fusion. Herein, we report a focused screen of these OA saponins using an efficient S/HIV pseudotyping system with the aim of obtaining potent anti-SARS-CoV-2 inhibitors. This screen identified two potent SARS-CoV-2 entry inhibitors **1** and **2** (Fig. 1B). Notably, 3β-*O*-[2, 4-di-*O*-(α-L-rhamnopyranosyl)-β-D-glucopyranosyl]-olean-12-en-28-oic acid benzyl ester (**2**) showed good inhibition toward SARS-CoV-2 with an IC_{50} value of 16.75 μM *in vitro* though having moderate cytotoxicity. Then optimization of **2** led to a series of novel SARS-CoV-2 entry inhibitors devoid of cytotoxicity. Furthermore, mechanism studies revealed that these OA saponins were identified as potential small-molecular fusion inhibitors that could inhibit SARS-CoV-2 infection through directly binding to the SARS-CoV-2 S2 subunit. This finding has provided validation for the continued development of the novel SARS-CoV-2 entry inhibitors based on pentacyclic triterpene saponins scaffolds.

2. Results and discussion

2.1. Screening potential OA saponins against pseudovirus model of SARS-CoV-2

Our previous screen of a pentacyclic triterpene saponin library identified a series of 3-*O*-β-chacotriosyl oleanane-type triterpenoids as potential H5N1 entry inhibitors [27,28]. In view of their significant inhibitory effect on IAV, we were sought to investigate whether the observed anti-IAV properties of these OA triterpenoids could extend to SARS-CoV-2 and translate into a shared mechanism that was capable of chemically antagonizing the SARS-CoV-2-cell fusion. Notably, one of the challenges of working with the highly pathogenic SARS-CoV-2 virus is that biosafety level 3 (BSL-3) facilities are required to handle this infectious virus due to the safety concerns. For studies of other highly pathogenic enveloped viruses such as HIV, H5N1 and EBOV/MARV, this obstacle has been circumvented by a surrogate pseudovirus (PsV) system, which can be widely utilized to not only identify antiviral agents but also study the entry mechanisms [33–35]. It has been proved that viral PsV systems for CoVs such as SARS-CoV and MERS-CoV are also valid surrogate assays [36,37]. Based on our previous study [13], we utilized a robust HIV pseudotype model with the SARS-CoV-2-S to screen the OA triterpenoids library for discovering entry inhibitors.

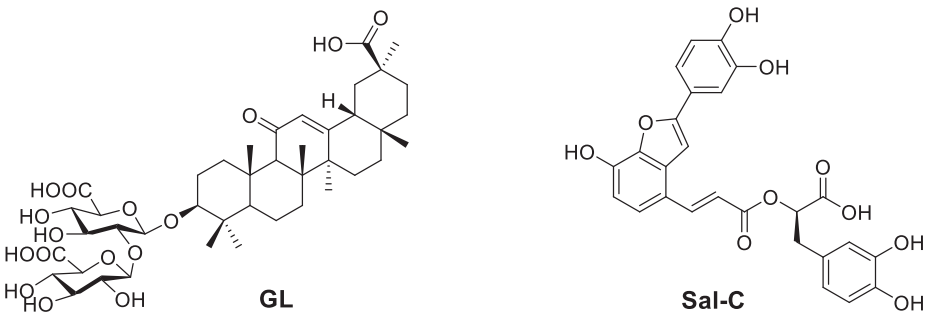

Fig. 1A. Representative antiviral agents as SARS-CoV-2 entry inhibitors.

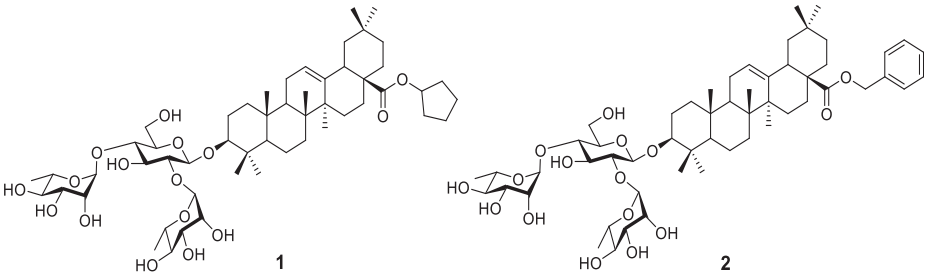

Fig. 1B. Potent SARS-CoV-2 entry inhibitors **1** and **2** from our screening.

This S/HIV pseudotype model allowed for direct comparison of SARS-CoV-2-S function with a common lentiviral core and reporter. Here all OA saponins were screened at 20 μM (Table S1), where hits with superior to 50% inhibition rate were retested to obtain accurate IC_{50} values. Interestingly, several hit compounds have been shown to inhibit the entry of SARS-CoV-2. Among them, **2** as a top hit, exhibited strongest inhibitory activity ($IC_{50} = 16.75$ μM) while it had moderate cytotoxicity against 293T-ACE2 cells. Structurally, the inhibitor **2** possesses a α-L-rhamnopyranosyl-(1 → 2)-[α-L-rhamnopyranosyl-(1 → 4)]-β-D-glucopyranosyl residue hydrophilic trisaccharide, named known as a chacotriose, attached to the hydrophobic aglycone OA via β-glycosidic linkage, followed by a benzyl side chain at 17-COOH of OA.

2.2. The preliminary structure-activity relationships (SARs)

As depicted in Table S1, these OA saponins were found to show a variety of inhibitory activities against SARS-CoV-2, strongly related to their structures. A preliminary meaningful structure-activity relationships (SARs) could be drawn from these observations to support further chemical optimization, as outlined in Fig. 2. We first analyzed the effect of branched trisaccharide scaffold of **2** on the inhibition. It was found that removal or positional change of its α-L-rhamnosyl residues as well as replacement of its α-L-rhamnosyl or β-D-glucopyranosyl residue with other monosaccharides, resulted in a significantly diminished inhibition and even a complete loss of potency. These results suggested that the chacotriosyl moiety was essential for inhibitor efficacy. Then evaluation focused on the side chain portion at C-28 position of OA indicated that esterification of the 17-COOH group of OA was helpful for inhibitory activity since deletion of the side chains led to a remarkably reduced inhibition toward SARS-CoV-2. Moreover the enhancement of potency appeared to be correlated to the length and bulk of the substituents at C-28 position of OA, signifying that these bulky side chains may extend to a potential auxiliary hydrophobic pocket to form hydrophobic interaction. Support for this hypothesis can be seen in the reported ester analogs **1** and **2** that dramatically enhance inhibitory activity in comparison with those bearing polar groups at C-28 position of OA. Among the COOH-substituted analogs, introduction of the benzyl group was superior to other alkyl groups, highlighting the superiority of the aryl side chain at C-28 position of OA, which probably allowed either favorable hydrophobic interactions or π-π interactions in the binding site.

2.3. New SARS-CoV-2 entry inhibitor design

Current work in our group is committed to the development of novel and potent SARS-CoV-2 entry inhibitors, resulting in the discovery of the high hit **2**. However, all these hits displayed moderate cytotoxicity against 293T-ACE2 cells, revealing that further modification might gain better SARS-CoV-2 entry inhibitors with increased potency and drug-like properties. To ablate toxic side effects, we incorporated in our chemical optimization campaign modifications to the preferred hit **2** by the bioisosteric replacement strategy. Accordingly, we attempted to adopt the amide linker to replace the ester linkage at C-17 position of OA, aiming to enhance selectivity index. In parallel to bioisosteric replacement to remove cytotoxicity, modifications were made to enhance affinity for the SARS-CoV-2-S. Our strategy here was to probe and optimize the side chain at 28-position of the hit **2** to identify detailed SARs that could be utilized to improve the potency against SARS-CoV-2, by introducing various phenyl and aralkyl groups at the 28-position Of OA via amide linker. Thus, we designed and synthesized a series of C-28 amide-substituted 3-*O*-β-chacotriosyl derivatives (Fig. 2, Table 1), anticipating that phenyl and aralkyl substituted groups at 28-position of OA would have sufficient length and size, relative flexibility, as well as appropriate hydrophobicity to bind effectively to the potential hydrophobic

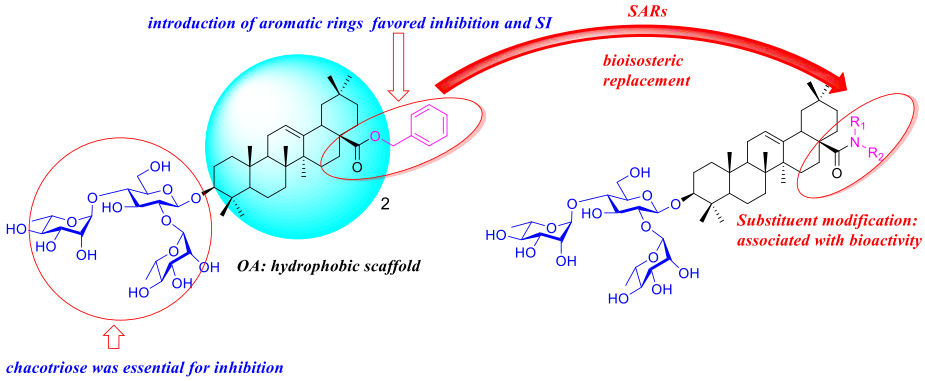

Fig. 2. The preliminary SARs and design strategy of OA saponins derivatives against SARS-CoV-2.

Table 1
Inhibitory activities of saponins **12a**-**12p** against infection of 293T-ACE2 cells by SARS-CoV-2 PsV.

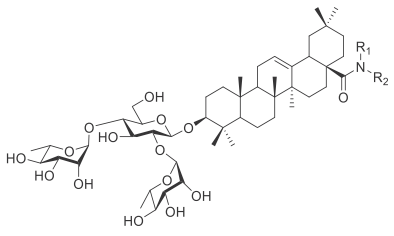

Comp.	R_1	R_2	IC_{50} (μM)	CC_{50} (μM)	SI
12a	H	phenyl	18.12 ± 1.28	33.46 ± 1.31	1.85
12b	H	2-methoxyphenyl	5.54 ± 0.45	31.24 ± 1.63	5.64
12c	H	3-methoxyphenyl	8.33 ± 0.99	>100.00	>12.00
12d	H	4-methoxyphenyl	9.97 ± 1.09	>100.00	>10.03
12e	H	2-chlorophenyl	6.27 ± 0.84	31.74 ± 1.11	5.06
12f	H	benzyl	4.37 ± 0.82	>100.00	>22.88
12g	H	2-pyridylmethyl	>20.00	NT	NT
12h	H	2-furylmethyl	>20.00	NT	NT
12i	H	2-thienylmethyl	5.89 ± 0.78	34.87 ± 1.32	5.92
12j	Me	benzyl	7.76 ± 0.69	37.56 ± 1.22	4.84
12k	H	2-fluorobenzyl	5.68 ± 0.78	>100.00	>17.61
12l	H	2-chlorobenzyl	6.32 ± 1.11	>100.00	>15.82
12 m	H	2-bromobenzyl	9.57 ± 0.65	>100.00	>8.51
12n	H	2-methoxybenzyl	16.75 ± 1.77	33.42 ± 1.02	2.00
12°	H	2-phenylethyl	7.37 ± 0.81	>100.00	>13.57
12p	H	3-phenylpropyl	13.06 ± 0.66	>100.00	>7.66
2			16.75 ± 1.11	21.63 ± 1.37	1.29
Sal-C			3.85 ± 0.38	>100.00	>25.97

IC_{50}: 50% inhibitory concentration.
CC_{50}: 50% cellular cytotoxicity concentration.
SI: selectivity index as CC_{50}/IC_{50}.

pocket. Given the importance of the benzyl group as an excellent privileged moiety in our preliminary screening data, we inferred reasonably that these design and optimization strategies would be fruitful.

2.4. Chemistry

To investigate substitutions at 28-position of the OA scaffold, a set of OA saponins amide analogs **12a**-**12p** were synthesized, containing various aryl moieties, as shown in Scheme 1. Allylation of commercially available OA with allyl bromide and potassium carbonate in DMF was performed to yield **3**. Subsequent glycosylation of **3** with the known 2,3,4,6-tetra-*O*-benzoyl-D-glucopyranosyl trichloroacetimidate (**4**) [34] in the presence of TMSOTf afforded the complete β-stereoselectivity product **5** that was attributed to the participation of the neighboring group in a stereoselective reaction at C-2 position in Glu. Removal of all the Bz protecting groups was performed with sodium methoxide in methanol to furnish the intermediate **6**. Then regioselective protection of C-6-OH and C-3-OH in Glu with pivaloyl (Piv) group was completed using pivaloyl chloride, leading to the important intermediate **7**. Synthesis of the trisaccharide saponin **9** was performed via a coupling reaction with **7** and the known donor 2,3,4-tri-*O*-acetyl-L-rhamnopyranosyl trichloroacetimidate (**8**) [38] by means of a similar TMSOTf-catalyzed glycosylation procedure, followed by deprotection of the Ac and Piv groups using NaOH. Then hydrogenolysis of Allyl moiety in **9** was completed using palladium chloride dissolved in THF-MeOH to yield **10**. Next, the obtained **10** was subjected to esterification reaction with acetic anhydride in the presence of DMAP to generate the key intermediate **11**. The sequence of acyl chloride formation, installation of a variety of amines by utilizing the traditional condensation procedure, and final removal of Ac groups was followed to produce the desired title saponins **12a**-**12p**, respectively.

2.5. Inhibition of the infection of SARS-CoV-2 pseudovirus

All title saponins **12a**-**12p** were tested in 293T-ACE2 cells infected by a SARS-CoV-2-S/HIV pseudotype virus containing a luciferase reporter gene, while VSV-G/HIV pseudoviral transduction was used as a specificity control to exclude inhibitory effect on post-entry for HIV infection. The biological data were summarized in Table 1. **Sal-C**, a small molecule entry inhibitor previously shown to target SARS-CoV-2-S [23], was used as the positive control in this assay. As shown in Table 1, all the saponins except **12g** and **12h** displayed inhibition against SARS-CoV-2 pseudovirus with a potency ranging from moderate (IC_{50} > 10 μM) to potent (IC_{50} < 10 μM).

Among them, **12f** exhibited the strongest inhibitory activity in a dose-dependent manner (Fig. 3A) with an IC_{50} value of 4.37 μM on 293T-ACE2 cells stably expressing human-ACE2, while no inhibition was observed on VSV-G pseudoviral transduction (Fig. 3A). Moreover **12f** showed negligible cytotoxicity against 293T-ACE2 cells (Fig. 3B). Likewise, other representative saponins **12b**, **12i** and **12k** showed significant inhibitory activity (IC_{50} < 6 μM, Table 1) but had no effect on VSV-G enveloped pseudovirus (Fig. S1, SI), suggesting that saponins were determined to inhibit the entry of SARS-CoV-2 PsV on 293T-ACE2 cells. Based on these results, we inferred that saponins **12a**-**12p** might block the entry of SARS-CoV-2 virus by targeting S protein, the only glycoprotein enveloped in the pseudovirus system. Support for this hypothesis can be seen in the saponin **12f** that showed strong binding affinity to S-trimer of SARS-CoV-2 with a K_D value of 0.94 μM on the basis of a surface plasmon resonance (SPR) assay (Fig. 3C).

Taking into account both potency and selectivity index, **12f** stood out among all title saponins evaluated, displaying excellent anti-SARS-CoV-2 activity and low cytotoxicity to 293T-ACE2 cells, which could be chosen as the lead compound for SARS-CoV-2 entry inhibitors.

2.6. Further SARs development

The goal of this SARs was to improve anti-SARS-CoV-2 activity observed with the hit **2** and explore the significance of amide substitutions at 28-position of OA with respect to SARS-CoV-2 inhibition and selectivity index. As expected, replacement of the ester with its bioisoster amide led to increased inhibition while little cytotoxic activity toward 293T-ACE2 cells (Table 1). It started with the replacement of the benzyl ester in hit **2** with aryl amide to vary the amine substituent. Phenyl amide analogs **12a**-**12e** demonstrated high potency against SARS-CoV-2 with IC_{50} < 20 μM, suggesting that substitutions at 28-position bearing highly hydrophobic and aromatic nature are preferred that was consistent with earlier finding. To confirm the advantage of substituents introduced to the 28-position of OA, **12a** was synthesized to represent the minimal scaffold without substituents attached. It was found that substitution with a phenyl ring (**12a**) resulted in the similar inhibition but slight decreased cytotoxicity compared to **2**. Interestingly, decoration of the phenyl substituents (**12b**-**12e**) led to markedly improved inhibition toward SARS-CoV-2 compared to **12a**, revealing the importance of structural modifications of phenyl ring for antiviral activity. In comparison to the unsubstituted derivative **12a**, antiviral activity was remarkably improved when a methoxy group or chlorine atom was attached to the *ortho*-position of the phenyl ring while keeping the similar cytotoxicity. In contrast, the attachment of methoxy group to the phenyl ring at the *meta*- or *para*-position resulted in enhanced potency and selectivity

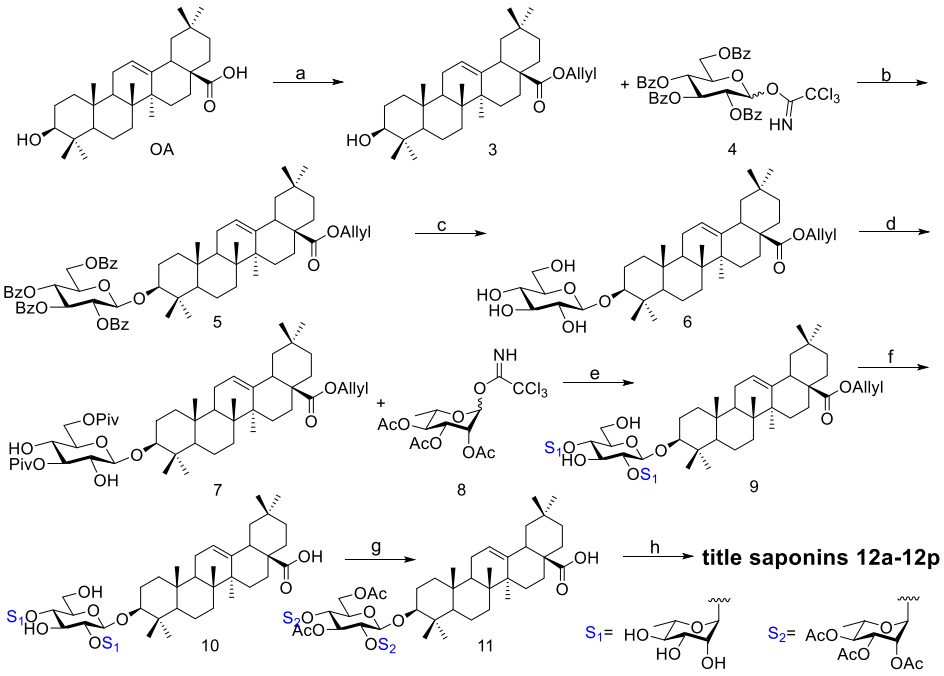

Scheme 1. Reagents and conditions: (a) AllylBr, K_2CO_3, DMF; (b) TMSOTf, CH_2Cl_2; (c) MeONa, CH_3OH; (d) PivCl, pyridine; (e) (i) TMSOTf, CH_2Cl_2; (ii) MeONa, MeOH; (f) $PdCl_2$, MeOH-THF; (g) Ac_2O, DMAP, pyridine; (h) (i) $(COCl)_2$, CH_2Cl_2; (ii) aromatic or aromatic alkyl amines, Et_3N, CH_2Cl_2; (iii) MeONa, MeOH.

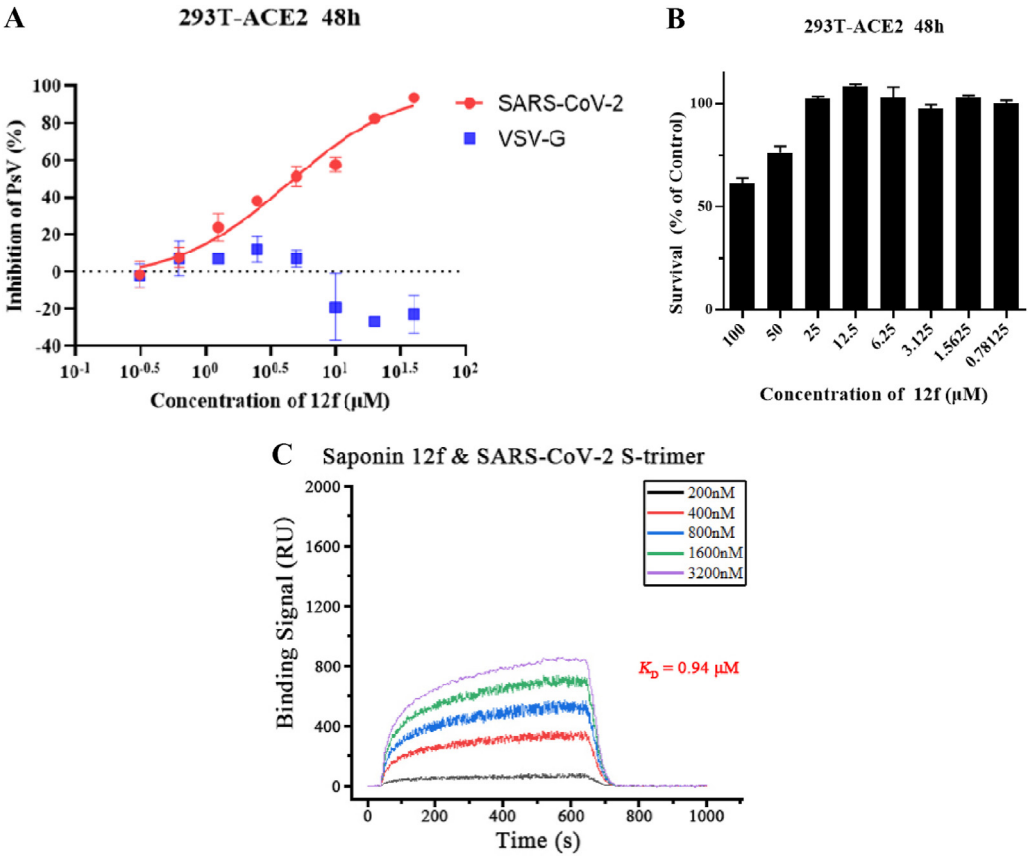

Fig. 3. (A) Dose-response curve for saponin **12f** in the antiviral assay against SARS-CoV-2 PsV and VSV-G PsV. (B) Cytotoxicity of saponin **12f** against 293T-ACE2 cells. (C) SPR analysis of the interaction between **12f** with SARS-CoV-2 S-trimer.

index though with slightly less intensity than the substituted at the *ortho*-position.

Next, we focused our attention on novel aralkyl-substituted derivatives (**12f**-**12p**) at C-28 position in which the phenyl group of **12a** was replaced with relatively long and flexible aralkyl groups containing one to three methylene bridges to probe the effect of length and steric bulk at this position. Encouragingly, a 28-benzyl-substituted analog **12f** is significantly more potent than **12a**, with a good IC_{50} value of 4.37 μM and high selectivity index (>22.88). This data revealed that addition of a methylene bridge was beneficial to better flexibility to adapt to the cavity in SARS-CoV-2-S. Inspired by those results, we then employed a bioisosterism strategy to design heteroaromatic aimde derivatives **12g**-**12i**, with the aim of improving the antiviral potency. However, a pyridine-ring analogue of **12g** showed a loss of potency against SARS-CoV-2, possibly owing to addition of a polar group to the core of hydrophobic ring, in accordance with the above-established SARs. Likewise, 2-furylmethylsubstituted analogue **12h** also lacked potency. Interestingly, the anti-SARS-CoV-2 potency of 2-thienyl methylsubstituted **12i** was not significantly right-shifted in relation to **12f**, in spite of high cytotoxicity. The impact of N, N-disubstitution was determined with compound **12j**. Unfortunately, addition of a methyl moiety at N group on our scaffold led to reduced inhibition of SARS-CoV-2 but stronger cytotoxicity compared to the corresponding monosubstituted **12f**.

Given that the N-monosubstituted **12f** with the benzyl substituent turned out to be the most potent inhibitor in this subseries **12f**-**12j**, we chose to explore some further modifications targeting the benzyl ring such as the introduction at *ortho*-position of halogen atoms, as in saponins **12k**-**12m**, introduction of methoxy groups, as in compound **12n**, and the introduction of one or two methyl groups in the linker, as in saponins **12o**-**12p**. Considering the inhibitory activity of saponins **12k**-**12n**, it is noted that substitutions in the benzyl ring gave less active compounds relative to the unsubstituted analog **12f**. However, some SARs were identified in this series. In general, the halogen substitutions in the benzyl ring did not contribute to the antiviral activity. Despite a fluorine derivative **12k** (IC_{50} = 5.68 μM) showed the comparable potency with **12f**, a reduction in the antiviral activity was observed with the increased atomic radius of their halogen atoms attached to *ortho*-position in the benzyl ring. Also, the introduction of a methoxy group at *ortho*-position in the benzyl ring (**12n**) was unfavorable (IC_{50} = 16.75 μM), conversely coupled with improved cytotoxicity, which supported the electronic characteristics of these groups positively influences inhibitory activity. It seemed that increasing number of methylene has a negative effect on the potency. For example, replacement with a two-carbon chains between the phenyl moiety and the amide, as in **12o** (IC_{50} = 7.37 μM), led to a slight reduction in potency, while a longer linker, as in **12p** (IC_{50} = 13.06 μM), caused a 3-fold drop in potency compared to **12f**. These results suggest that either too large (phenylpropyl) or too rigid (phenyl) N-substituted groups are unfavorable for inhibitory activity toward SARS-CoV-2. As observed, not only the electronic characteristics of substituents in aromatic ring but also hydrophobic effects of the substituents at 28-position of OA are responsible for the efficiency of anti-SARS-CoV-2 activity.

2.7. Confirmation of the lead *12f* against infectious SARS-CoV-2

To validate potency of the lead **12f**, we tested it against wild-type SARS-CoV-2 (wuhan-HU-1 variant) strain where chloroquine (CQ) was used as a positive control [23]. Specifically, we examined the protective effects of **12f** on Vero-E6 cells from highly pathogenic SARS-CoV-2 virus infection via observing virus distribution profile reflected by viral nucleoprotein (NP) expression utilizing immunofluorescence microscopy (IFA) at 48 hpi. As shown in Fig. 4A, compound **12f** was capable of inhibiting SARS-CoV-2 infection in a dose-dependent manner as do the control group, confirming the anti-SARS-CoV-2 efficacy of **12f** and the validity of the pseudotype model. Consistently, **12f** exhibited the potent antiviral activity with an IC_{50} value of 0.97 μM as observed in Fig. 4B. Moreover, **12f** had negligible cytotoxicity against Vero-E6 cells (Fig. 4C) that was agreement with that in 293T-ACE2 cells. Collectively, the saponin **12f** was an improved lead compound in relation to the hit **2**, which was a good candidate as a potential antiviral treatment for SARS-CoV-2.

2.8. *12f* does not block binding with S1 subunit of SARS-CoV-2-S

The spike protein of SARS-CoV-2 is consisted of S1 and S2 subunits, which is responsible for recognition of host cells and virus-cell membrane fusion, respectively. To investigate the region (s) in S protein of **12f**, we conducted a Co-Immunoprecipitation (Co-IP) assay to detect the effect of **12f** on SARS-CoV-2 S1 subunit binding to human ACE2. As shown in Fig. 5A, compound **12f** displayed no effect on inhibition of SARS-CoV-2 S binding to the ACE2 receptor, demonstrating that SARS-CoV-2 S1 subunit was not a potential binding site of **12f**. Consistent with the Co-IP results, **12f** showed much lower binding affinity with S1 subunit (at millimolar level, Fig. 5B) compared to that with S protein based on SPR. This data further confirmed that **12f** did not mainly target S1 subunit of SARS-CoV-2. Additionally, we determined the binding affinities between **12f** and S2 subunit. On the contrary, **12f** exhibited a more than 1000-fold higher affinity with S2 subunit (K_D = 2.16 μM, Fig. 5C) in relation to S1 subunit (K_D = 3.69 mM, Fig. 5B). Taken together, these data suggested that **12f** has the tendency to bind to the regions in S2 subunit of SARS-CoV-2 S protein.

2.9. *12f* could block cell-cell fusion mediated by SARS-CoV-2 S protein

With the aim of further confirming mode of action of **12f**, we next utilized the cell-cell fusion assay mediated by SARS-CoV-2 S protein to probe whether **12f** is a potential fusion inhibitor based on our previous studies on seeking for h-CoVs fusion inhibitors [39]. As shown in Fig. 6, **12f** could remarkably inhibit the membrane fusion of Vero-E6 cells mediated by SARS-CoV-2 S protein in a dose-dependent manner, of which the result was consistent with our SPR data. On the basis of these results, we inferred that **12f**, as a potential small-molecular fusion inhibitor, could inhibit SARS-CoV-2 infection by binding to the conserved SARS-CoV-2 S2 subunit to prevent membrane fusion, thus blocking viral entry, although the specific binding characteristics of SARS-CoV-2 S2 subunit with **12f** remained to be explored.

3. Conclusion

This study presented here discovered several new SARS-CoV-2 entry inhibitors, via a focused screen of the OA saponin library against pseudotyped SARS-CoV-2. Based on the structure of the top hit **2**, rational drug design and subsequent chemical optimization resulted in the development of a potent set of SARS-CoV-2 fusion inhibitors with 3-*O*-β-chacotriosyl OA amide skeleton. The lead compound **12f** had favorable SI values when tested with infectious SARS-CoV-2. Intensive SARs indicated that the chacotriosyl moiety was indispensable for efficacy and introduction of a hydrophobic aromatic ring through a flexible amide linker at 28-position of OA favored antiviral activity and selectivity index. Utilizing the Co-IP assay, SPR analysis and cell-cell fusion studies, we confirmed that the lead **12f** was capable of direct binding to SARS-CoV-2 S2 subunit

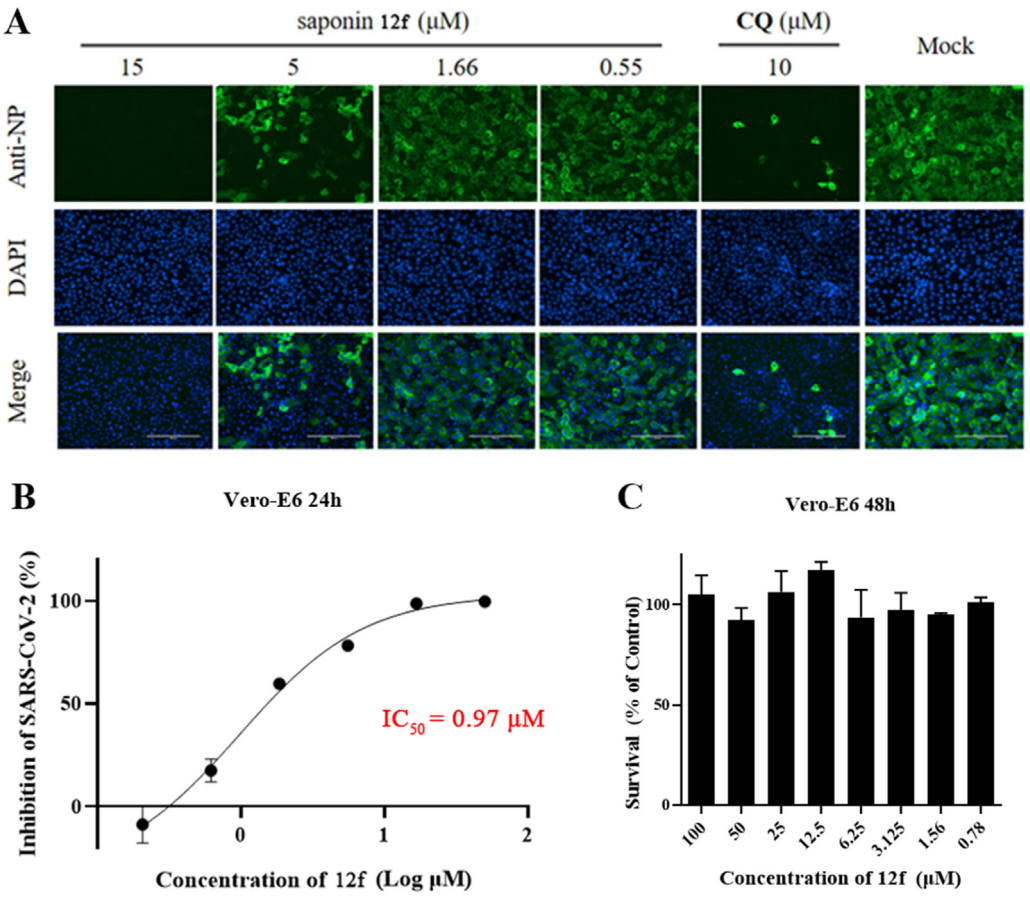

Fig. 4. (A) Antiviral activity of **12f** against SARS-CoV-2 infection was detected by indirect immunofluorescence assay with chloroquine (CQ) as a positive control, scale bar = 200 μm. (B) Dose-response curve for **12f** in the authentic SARS-CoV-2 virus infection assay. (C) Cytotoxicity of **12f** against Vero-E6 cells.

to block membrane fusion. Overall, 3-*O*-β-chacotriosyl OA amide saponins represent a promising scaffold for the further development as a potential treatment for SARS-CoV-2 infections.

4. Experimental protocols

4.1. General methods

Solvents were purified in a conventional manner. Thin layer chromatography (TLC) was performed on precoated E. Merck silica gel 60 F254 plates. Flash column chromatography was performed on silica gel (200–300 mesh, Qingdao, China). ^{1}H NMR and ^{13}C NMR spectra were taken on a JEOL JNM-ECP 600 spectrometer with tetramethylsilane as an internal standard, and chemical shifts are recorded in ppm values. Mass spectra were recorded on a Q-TOF Global mass spectrometer.

4.2. 3-Hydroxy-olean-12-en-28-oic acid allyl ester (*3*)

To a solution of OA (2.00 g, 4.38 mmol) in dry DMF (50 mL) was added potassium carbonate (1.20 g, 8.76 mmol). After 4 h of stirring at r.t., allyl bromide (0.96 mL, 13.14 mmol) was added and the mixture was stirred for an additional 8 h. The solvents were evaporated *in vacuo* and the residue was dissolved in a mixture of CH_2Cl_2 (150 mL), washed with brine (2 × 100 mL). The organic layer was dried over anhydrous Na_2SO_4, filtered, and concentrated under diminished pressure. Recrystallization from EtOH provided **3** (2.00 g, 92%) as a colorless solid; m. p.: 220.8–222.3 °C; ^{1}H NMR (600 MHz, $CDCl_3$): δ 5.96–5.82 (m, 1H, C*H*=CH_2), 5.35–5.25 (m, 2H, C*H*=CH_2-1, H-12), 5.19 (d, 1H, *J* = 10.5 Hz, C*H*=CH_2-2), 4.51 (t, *J* = 5.3 Hz, 2H, OCH_2), 3.20 (dd, 1H, *J* = 11.1, 4.4 Hz, H-3), 2.87 (dd, 1H, *J* = 13.6, 3.9 Hz, H-18), 1.12, 0.97, 0.91, 0.89, 0.87, 0.76, 0.71 (each s, each 3H, each CH_3); ^{13}C NMR (150 MHz, $CDCl_3$): δ 177.4 (C-28), 143.7 (C-13), 132.5 (C-12), 122.4, 117.7, 79.0, 64.8, 55.2, 47.6, 46.7, 45.9, 41.7, 41.3, 39.3, 38.8, 38.4, 37.0, 33.9, 33.1, 32.7, 32.4, 30.7, 28.1, 27.7, 27.2, 25.9, 23.6, 23.4, 23.1, 18.3, 17.0, 15.6, 15.3; HRMS (ESI) *m/z* calcd for $C_{33}H_{53}O_3$ $[M+H]^+$ 497.3971, found 497.3978.

4.3. 3β-O-(2,3,4,6-tetra-O-benzoyl-β-D-glucopyranosyl)-olean-12-en-28-oic acid allyl ester (*5*)

To a solution of **3** (2.00 g, 4.03 mmol), 2,3,4,6-tetra-*O*-benzoyl-D-glucopyranosyl trichloroacetimidate (**4**) (3.59 g, 4.84 mmol) and 4 Å molecular sieves in dry CH_2Cl_2 was added TMSOTf (133 μL g, 0.60 mmol) at 0 °C under argon. The reaction mixture was stirred for 1 h and warmed to r.t. for 1 h. The reaction was quenched by Et_3N and concentrated. The residue was purified by silica gel column chromatography (petroleum ether-EtOAc, 6:1) to afford **5** (4.03 g, 93%) as a colorless solid; m. p.: 232.1–233.6 °C; ^{1}H NMR (600 MHz, $CDCl_3$): δ 8.04–8.00 (m, 2H, Ar–H), 7.96–7.89 (m, 4H, Ar–H), 7.86–7.81 (m, 2H, Ar–H), 7.57–7.46 (m, 3H, Ar–H), 7.45–7.32 (m, 7H, Ar–H), 7.29 (d, 2H, *J* = 7.9 Hz, Ar–H), 5.91 (t, 1H, *J* = 9.7 Hz, H-3′), 5.92–5.83 (m, 1H, C*H*=CH_2), 5.58 (t, 1H, *J* = 9.7 Hz, H-4′), 5.57 (dd, 1H, *J* = 9.8, 7.9 Hz, H-2′), 5.35–5.26 (m, 2H, C*H*=CH_2-1, H-12), 5.19 (dd, 1H, *J* = 10.4, 1.4 Hz, C*H*=CH_2-2), 4.85 (d, 1H, *J* = 7.9 Hz, H-1′), 4.62–4.49 (m, 4H, H-6′, OCH_2), 4.18–4.10 (m, 1H,

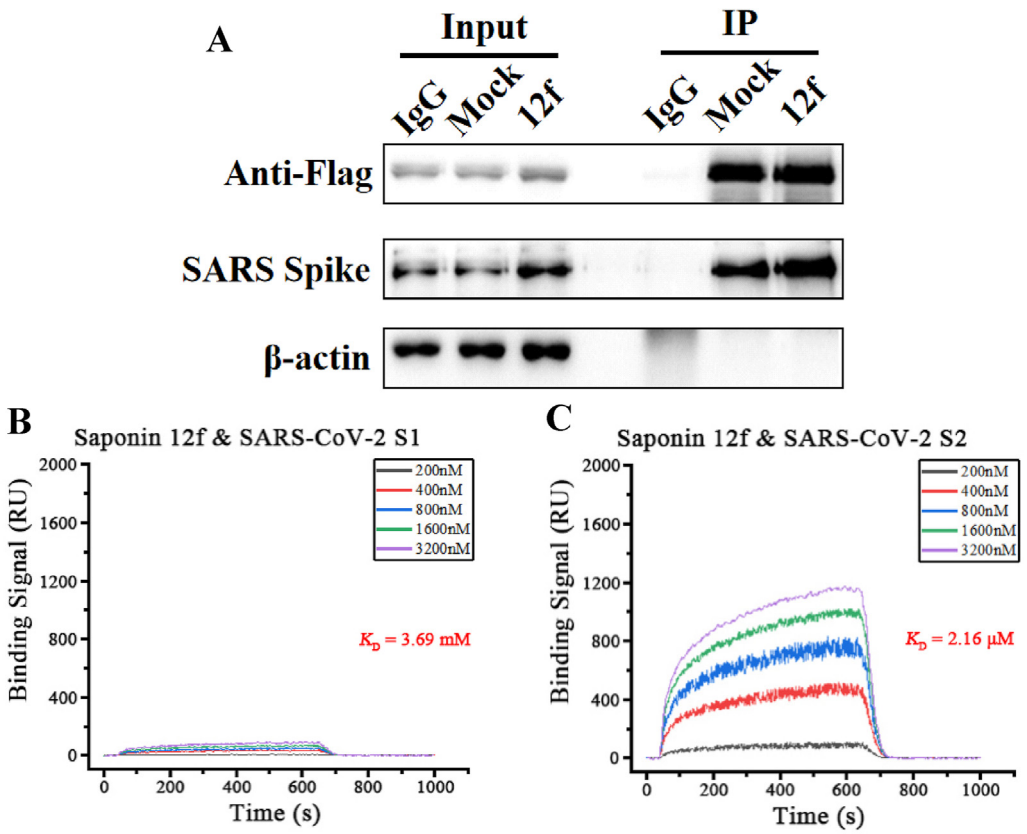

Fig. 5. (A) The binding of SARS-CoV-2 S protein and ACE2 (Anti-Flag) in the presence or absence of **12f** (40 μM) were detected by Co-IP assays. IgG was included as a negative control. (B–C) SPR analysis of the interaction between **12f** with SARS-CoV-2 S1 subunit (B) and S2 subunit (C).

H-5′), 3.10 (dd, 1H, J = 11.7, 4.5 Hz, H-3), 2.88 (dd, 1H, J = 13.7, 3.7 Hz, H-18), 1.09), 0.93, 0.91, 0.82, 0.68, 0.67, 0.62 (each s, each 3H, each CH_3); ^{13}C NMR (150 MHz, $CDCl_3$): δ 177.3 (C-28), 166.0, 165.9, 165.3, 165.0, 143.7 (C-13), 133.5, 133.2, 133.1 (two), 132.5 (C-12), 129.9 (two), 129.8 (two), 129.7 (five), 129.4, 128.8, 128.8, 128.4 (four), 128.3 (four), 122.4, 117.7, 103.3 (C-1′), 90.8, 73.0, 72.1, 72.0, 70.3, 64.8, 63.4, 55.4, 47.6, 46.7, 45.9, 41.6, 41.3, 39.3, 38.7, 38.2, 36.6, 33.9, 33.2, 32.6, 32.4, 30.7, 27.7 (two), 25.9, 25.8, 23.7, 23.4, 23.0, 18.1, 16.9, 16.2, 15.2; HRMS (ESI) *m/z* calcd for $C_{67}H_{79}O_{12}$ $[M+H]^+$ 1075.5505, found 1075.5546.

*4.4. 3β-O-(β-D-glucopyranosyl)-olean-12-en-28-oic acid allyl ester (**6**)*

Compound **5** (4.03 g, 3.75 mmol) was dissolved in CH_2Cl_2 and MeOH (V:V = 1:1, 80 mL) and then NaOMe was added until pH = 10, respectively. After stirred at r.t. overnight, the solution was neutralized with Dowex 50 × 8 (H^+) resin until pH = 7, filtered and concentrated *in vacuo*. Then the residue was purified by silica gel column chromatography (CH_2Cl_2–MeOH, 10:1) to give **6** (2.35 g, 95%) as a colorless solid; m. p.: 153.8–155.3 °C; ^{1}H NMR (600 MHz, $CDCl_3$): δ 5.98–5.86 (m, 1H, C*H*=CH_2), 5.38–5.28 (m, 2H, C*H*=CH_2-1, H-12), 5.23 (dd, 1H, J = 10.5, 1.2 Hz, C*H*=CH_2-2), 4.61–4.49 (m,

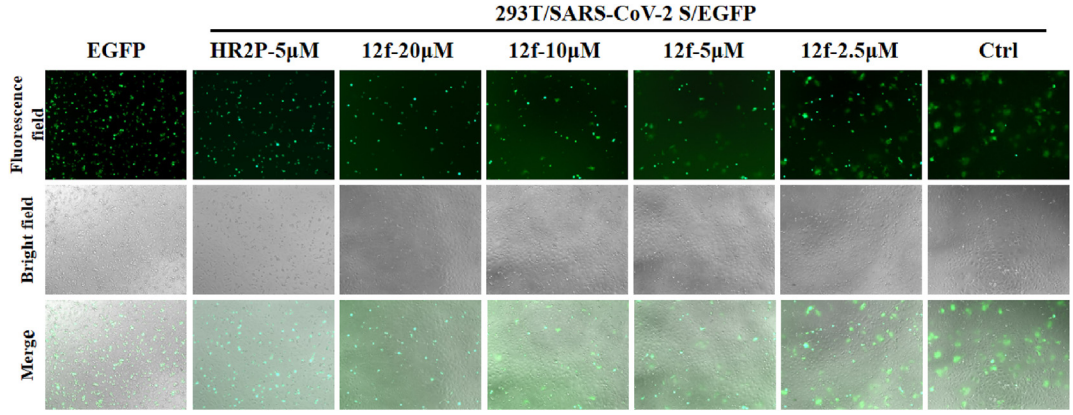

Fig. 6. The dose-dependent inhibitory efficacy of **12f** in the cell-cell fusion assay.

2H, OCH_2), 4.35 (d, 1H, J = 7.1 Hz, H-1′), 3.56–3.50 (m, 2H, H-6′), 3.65–3.56 (m, 1H, H-4′), 3.56–3.50 (m, 1H, H-3′), 3.47–3.38 (m, 1H, H-2′), 3.27 (d, 1H, J = 11.4 Hz, H-3), 3.20–3.10 (m, 1H, H-5′), 2.91 (dd, 1H, J = 13.3, 2.7 Hz, H-18), 1.14, 1.01, 0.95, 0.93, 0.91, 0.82, 0.74 (each s, each 3H, each CH_3); ^{13}C NMR (150 MHz, $CDCl_3$): δ 178.3 (C-28), 144.3 (C-13), 133.1 (C-12), 123.3, 117.6 (two), 106.1 (C-1′), 90.1, 77.6, 77.0, 75.0, 71.0, 65.4, 62.1, 56.4, 47.5, 46.5, 42.2, 42.1, 40.1, 39.5, 39.2, 37.2, 34.2, 33.4, 33.1, 32.9, 31.0, 28.1, 27.9, 26.4, 25.8, 23.9, 23.5, 23.3, 18.7, 17.2, 16.4, 15.4; HRMS (ESI) m/z calcd for $C_{39}H_{63}O_8$ $[M+H]^+$ 659.4478, found 659.4434.

4.5. 3β-O-(3,6-di-O-pivaloyl-β-D-glucopyranosyl)-olean-12-en-28-oic acid allyl ester (**7**)

To a cold solution of compound **6** (2.35 g, 3.56 mmol) in dry CH_2Cl_2 and pyridine (V:V = 1:1, 100 mL), pivaloyl chloride (2.19 mL, 17.8 mmol) dissolved in dry CH_2Cl_2 (5 mL) was added dropwise over a period of 10 min at −10 °C and the reaction mixture was allowed to stir for another 12 h. After the reaction was complete as judged by TLC, the mixture was concentrated *in vacuo*. Then the residue was diluted with EtOAc (100 mL) and washed with 1 M HCl (50 mL × 3), saturated aq $NaHCO_3$ (50 mL × 3), and brine (50 mL). The organic layer was dried over Na_2SO_4, filtered, and concentrated under diminished pressure. Purification of the crude reaction product by column chromatography on silica gel (petroleum ether-EtOAc, 3:1) furnished **7** (2.15 g, 73%) as a colorless solid; m. p.: 114.7–116.4 °C; ^{1}H NMR (600 MHz, $CDCl_3$): δ 5.93–5.84 (m, 1H, CH═CH_2), 5.30 (d, 2H, J = 17.7 Hz, CH═CH_2-1, H-12), 5.19 (d, 1H, J = 10.5 Hz, CH═CH_2-2), 4.88 (t, 1H, J = 9.2 Hz, H-3′), 4.52 (d, 1H, J = 5.1 Hz, OCH_2-1), 4.50 (d, 1H, J = 5.0 Hz, OCH_2-2), 4.45 (dd, 1H, J = 11.8, 1.9 Hz, H-6′-1), 4.40 (d, 1H, J = 7.8 Hz, H-1′), 4.17 (dd, 1H, J = 11.0, 8.0 Hz, H-6′-2), 3.63–3.49 (m, 2H, H-5′, H-4′), 3.44 (t, 1H, J = 9.2 Hz, H-2′), 3.14 (dd, 1H, J = 11.7, 4.2 Hz, H-3), 2.87 (dd, 1H, J = 13.7, 4.0 Hz, H-18), 1.23 (s, 9H, C(CH_3)$_3$), 1.19 (s, 9H, C(CH_3)$_3$), 1.11, 0.98, 0.91, 0.89, 0.88, 0.80, 0.71 (each s, each 3H, each CH_3); ^{13}C NMR (150 MHz, $CDCl_3$): δ 180.2 (C-28), 178.6, 177.4, 143.7 (C-13), 132.5 (C-12), 122.4, 117.7, 104.8 (C-1′), 90.3, 77.8, 74.1, 72.7, 70.1, 64.8, 63.8, 55.5, 47.6, 46.7, 45.9, 41.7, 41.3, 39.4, 39.0, 39.0, 38.8, 38.4, 36.7, 33.9, 33.1, 32.7, 32.4, 30.7, 28.3, 27.6, 27.2 (two), 27.1 (two), 26.9, 26.5, 25.9, 25.8, 23.6, 23.4, 23.0, 18.2, 16.9, 16.6, 15.3; HRMS (ESI) m/z calcd for $C_{49}H_{79}O_{10}$ $[M+H]^+$ 827.5540, found 827.5540.

4.6. 3β-O-[2,4-di-O-(α-L-rhamnopyranosyl)-β-D-glucopyranosyl]-olean-12-en-28-oic acid allyl ester (**9**)

To a mixture of **7** (2.15 g, 2.60 mmol) and 4 Å molecular sieves in dried CH_2Cl_2 (50 mL) at 0 °C under argon was added TMSOTf (141 μL, 0.78 mmol), followed by a solution of 2,3,4-tri-*O*-acetyl-L-rhamnopyranosyl trichloroacetimidate (**8**) (5.65 g, 13 mmol) in CH_2Cl_2 (5 mL). After stirring at 0 °C for 2 h and then at r.t. for 1 h, the reaction was quenched with triethylamine. The solid was filtered, and the filtrate was concentrated under vacuum to give a yellow oil. Next the residue was subjected to column chromatography on silica gel (EtOAc-petroleum ether, 1:4) to provide the crude trisaccharide, which was dissolved in THF-CH_3OH-H_2O (V:V:V = 1:1:1, 90 mL) and then NaOH (1.46 g, 36.40 mmol) was added. After stirred at 50 °C overnight, the solution was neutralized with Dowex 50 × 8 (H^+) resin until pH = 7, filtered and concentrated *in vacuo*. The crude product was purified by silica gel column chromatography (CH_2Cl_2–MeOH, 6:1) to afford **9** (1.82 g, 70%, for two steps) as a colorless solid; m. p.: 252.3–254.1 °C; ^{1}H NMR (600 MHz, CD_3OD): δ 5.99–5.86 (m, 1H, CH═CH_2), 5.36 (dd, J = 3.8, 1.5 Hz, 2H), 5.33–5.24 (m, 2H, CH═CH_2-1, H-12), 5.22 (dd, 1H, J = 10.5, 1.3 Hz, CH═CH_2-2), 5.00 (d, 1H, J = 1.4 Hz, Rha-H-1), 4.85 (d, 1H, J = 1.2 Hz, Rha-H-1), 4.53 (d, 1H, J = 5.6 Hz, OCH_2-2), 4.51 (d, 1H, J = 5.5 Hz, OCH_2-2), 4.43 (d, 1H, J = 7.7 Hz, H-1), 4.02–3.95 (m, 2H), 3.95–3.87 (m, 1H), 3.84 (dd, 1H, J = 2.9, 1.7 Hz, Rha-H-2), 3.80 (dd, 1H, J = 12.7, 1.8 Hz, H-6′-1), 3.75 (dd, 1H, J = 9.6, 3.4 Hz, Rha-H-3), 3.69 (dd, 1H, J = 8.3, 3.6 Hz, Rha-H-3), 3.66–3.60 (m, 2H), 3.56 (t, J = 8.9 Hz, 2H), 3.47–3.35 (m, 4H), 3.16 (dd, 1H, J = 11.6, 4.0 Hz, H-3), 2.89 (dd, 1H, J = 13.6, 3.9 Hz, H-18), 1.27 (d, 3H, J = 6.3 Hz, Rha-H-6), 1.21 (d, 3H, J = 6.2 Hz, Rha-H-6), 1.16, 1.05, 0.94, 0.34, 0.92, 0.86, 0.75 (each s, each 3H, each CH_3); ^{13}C NMR (150 MHz, CD_3OD): δ 176.3 (C-28), 142.2 (C-13), 131.0 (C-12), 121.2, 115.5, 102.8 (C-1′), 100.3 (Rha-C-1), 99.3 (Rha-C-1), 87.6, 77.6, 76.5, 75.4, 73.7, 71.5, 71.2, 70.9, 70.3, 69.7, 69.4, 69.3, 68.0, 67.3, 66.5, 63.3, 59.2, 54.6, 40.1, 40.1, 38.0, 37.5, 37.3, 35.1, 32.1, 31.3, 31.0, 30.8, 28.9, 26.0, 25.8, 24.5, 23.8, 21.8, 21.4, 21.3, 16.6, 15.4, 15.3, 15.2, 15.0, 14.5, 13.4; HRMS (ESI) m/z calcd for $C_{51}H_{83}O_{16}$ $[M+H]^+$ 951.5527, found 951.5585.

4.7. 3β-O-[2,4-di-O-(α-L-rhamnopyranosyl)-β-D-glucopyranosyl]-olean-12-en-28-oic acid (**10**)

Compound **9** (1.82 g, 1.82 mmol) was dissolved in MeOH and CH_2Cl_2 (V:V = 1:1, 40 mL), $PdCl_2$ (161 mg, 0.91 mmol) was then added. The mixture was vigorously stirred at r.t. for 3 d and then filtered over a celite pad and concentrated under vacuum. The crude product was subjected to column chromatography on silica gel (CH_2Cl_2–MeOH, 5:1) to provide **10** (1.49 g, 90%) as a colorless solid; m. p.: 201.6–203.4 °C; ^{1}H NMR (600 MHz, CD_3OD): δ 5.38 (s, 1H, Rha-H-1), 5.26 (t, 1H, J = 3.0 Hz, H-12), 4.87 (s, 1H, Rha-H-1), 4.44 (d, 1H, J = 7.8 Hz, H-1′), 4.0–43.97 (m, 1H), 3.98 (dd, 1H, J = 3.2, 1.8 Hz, Rha-H-2), 3.94–3.91 (m, 1H), 3.85 (dd, 1H, J = 3.2, 2.0 Hz, Rha-H-2), 3.82 (d, 1H, J = 10.8 Hz, H-6′-1), 3.76 (dd, 1H, J = 9.5, 3.3 Hz, Rha-H-3), 3.68 (dd, 1H, J = 12.0, 4.0 Hz, H-6′-2), 3.64 (dd, 1H, J = 9.3, 3.2 Hz, Rha-H-3), 3.60 (t, 1H, J = 8.7 Hz), 3.55 (t, 1H, J = 8.8 Hz), 3.46 (t, 1H, J = 8.2 Hz), 3.42 (t, 1H, J = 9.3 Hz), 3.38 (t, 1H, J = 9.5 Hz), 3.18 (dd, 1H, J = 11.6, 4.0 Hz, H-3), 2.86 (dd, 1H, J = 13.9, 3.7 Hz), 1.28 (d, 3H, J = 6.2 Hz, Rha-H-6), 1.22 (d, 3H, J = 6.2 Hz, Rha-H-6), 1.17, 1.06, 0.96, 0.95, 0.92, 0.87, 0.83 (each s, each 3H, each CH_3); ^{13}C NMR (150 MHz, CD_3OD): δ 180.8 (C-28), 143.8 (C-13), 122.2 (C-12), 104.0 (C-1′), 101.6 (Rha-C-1), 100.6 (Rha-C-1), 89.0, 79.0, 77.8, 76.7, 75.0, 72.5, 72.3, 71.0, 70.7, 70.6, 69.4, 68.6, 60.6, 55.9, 46.3, 45.9, 41.5, 41.3, 39.2, 38.8, 38.7, 36.5, 33.5, 32.6, 32.4, 32.2, 30.2, 27.4, 27.1, 25.8, 25.0, 23.1, 22.7, 22.6, 17.9, 16.6, 16.5, 16.3, 15.8, 14.6; HRMS (ESI) m/z calcd for $C_{48}H_{79}O_{16}$ $[M+H]^+$ 911.5228, found 911.5283.

4.8. 3β-O-[2,4-di-O-(2,3,4-tri-O-acetyl-α-L-rhamnopyranosyl)-β-(3,6-two-O-acetyl)-D-glucopyranosyl]-olean-12-en-28-oic acid (**11**)

A mixture of **10** (1.49 g, 1.64 mmol), Ac_2O (2.48 mL, 26.24 mmol) and DMAP (300 mg, 2.46 mmol) in pyridine (20 mL) was stirred at r.t. overnight. The mixture was concentrated and dissolved in CH_2Cl_2 (100 mL), then washed with 1 M HCl (3 × 50 mL), saturated $NaHCO_3$ (3 × 50 mL) and brine (2 × 50 mL). The organic layer was dried over anhydrous Na_2SO_4, filtered, and concentrated *in vacuo*. Then the residue was purified by silica gel column chromatography (petroleumether-EtOAc, 2:1) to produce **11** (1.89 g, 93%) as a colorless solid; m. p.: 151.7–153.4 °C; ^{1}H NMR (600 MHz, $CDCl_3$): δ 5.29 (t, 1H, J = 3.2 Hz, H-12), 5.25–5.23 (m, 2H), 5.18 (dd, 1H, J = 10.2, 3.2 Hz, Rha-H-3), 5.12 (dd, 1H, J = 3.2, 1.6 Hz, Rha-H-2), 5.06–5.00 (m, 4H), 4.80 (d, 1H, J = 1.8 Hz, Rha-H-1), 4.55 (d, 1H, J = 7.7 Hz, H-1′), 4.48 (dd, 1H, J = 12.2, 1.8 Hz, H-6-1′), 4.28 (dd, 1H, J = 12.3, 4.2 Hz, H-6-2′), 4.24–4.21 (m, 1H), 3.88–3.84 (m, 1H), 3.78 (t, 1H, J = 9.4 Hz), 3.68 (t, 1H, J = 8.4 Hz), 3.63–3.61 (m, 1H), 3.16 (dd, 1H, J = 11.6, 4.0 Hz, H-3), 2.84 (dd, 1H, J = 13.4, 4.2 Hz, H-18), 2.14, 2.14, 2.13, 2.10, 2.05, 2.02, 1.99, 1.98 (each s, each 3H, each CH_3CO), 1.17 (d, 6H, J = 6.2 Hz, 2 × Rha-H-6), 1.14, 1.04, 0.94, 0.92, 0.91, 0.81, 0.76 (each s, each 3H, CH_3); ^{13}C NMR (150 MHz, $CDCl_3$): δ 182.7 (C-

28), 170.6, 170.2, 170.1, 170.0 (three), 169.9, 169.6, 143.4 (C-13), 122.5 (C-12), 103.6 (C-1′), 99.5 (Rha-C-1), 97.1 (Rha-C-1), 89.9, 78.0, 75.6, 75.4, 72.1, 71.1, 70.5, 69.9, 69.7, 68.6, 68.5, 67.9, 66.7, 62.2, 55.9, 47.6, 46.5, 45.8, 41.6, 41.1, 39.3, 39.0, 38.9, 36.7, 33.8, 33.1, 32.6, 32.5, 30.7, 29.7, 27.8, 27.6, 26.0, 25.9, 24.5, 23.6, 23.4, 22.9, 21.4, 20.9 (two), 20.8 (two), 20.7 (two), 18.2, 17.2, 17.1, 16.9, 16.3, 16.2, 15.4; HRMS (ESI) *m/z* calcd for $C_{64}H_{95}O_{24}$ $[M+H]^+$ 1247.6149, found 1248.6047.

4.9. General procedure for the preparation of **12a-12p**

To a solution of **11** (1.0 mmol) in dry CH_2Cl_2 (20 mL) was added oxalyl chloride (1 mL), and the mixture was allowed to stir at r.t. for 24 h under argon. Next, the dichloromethane was removed via vacuum. The prepared acid chloride was dissolved in dry CH_2Cl_2 (30 mL) and put under a nitrogen gas atmosphere. The appropriate amine (2.0 mmol) was then added followed by triethylamine (4.0 mmol). The resulting mixture was stirred at r.t. for 5 h and then concentrated *in vacuo*. The obtained residue was dissolved in MeOH and CH_2Cl_2 (*V*:*V* = 2:1, 15 mL) and then NaOMe was added until pH = 10. After stirred at r.t. for 3 h, the solution was neutralized with Dowex 50 × 8 (H^+) resin until pH = 7, filtered and concentrated in *vacuo*. Then the crude product was purified by silica gel column chromatography (CH_2Cl_2—MeOH, 6:1) to provide **12a-12p**, respectively.

4.9.1. N-{3β-O-[2, 4-di-O-(a-L-rhamnopyranosyl)-β-D-glucopyranosyl]-olean-12-en-28-oyl}-aniline (**12a**)

Compound **12a** was obtained as a white solid in 92% yield; m. p.: 197.1—198.3 °C; ^{1}H NMR (600 MHz, CD_3OD): δ 7.46 (d, 2H, *J* = 7.7 Hz, Ar—H), 7.29 (t, 2H, *J* = 7.9 Hz, Ar—H), 7.09 (t, 1H, *J* = 7.4 Hz, Ar—H), 5.45 (t-like, 1H, H-12), 5.36 (d, 1H, *J* = 1.0 Hz, Rha-H-1), 4.42 (d, 1H, *J* = 7.7 Hz, H-1′), 3.91 (dd, 1H, *J* = 9.5, 6.2 Hz, Rha-H-4), 3.84 (dd, 1H, *J* = 2.9, 1.8 Hz, Rha-H-2), 3.80 (d, 1H, *J* = 11.8 Hz, 1.4 Hz, H-6′-1), 3.74 (dd, 1H, *J* = 9.6, 3.4 Hz, Rha-H-3), 3.66 (dd, 1H, *J* = 12.1, 4.0 Hz, H-6′-2), 3.63 (dd, 1H, *J* = 9.5, 3.3 Hz, Rha-H-3), 3.60—3.56 (m, 1H), 3.54 (t, 1H, *J* = 9.1 Hz), 3.46—3.36 (m, 3H), 3.16 (dd, 1H, *J* = 11.7, 4.2 Hz, H-3), 2.95 (dd, 1H, *J* = 13.0, 3.3 Hz, H-18), 1.26 (d, 3H, *J* = 6.2 Hz, Rha-H-6), 1.20 (d, 6H, *J* = 6.0 Hz, Rha-H-6, CH_3), 1.04, 0.98, 0.94, 0.92, 0.84, 0.74 (each s, each 3H, each CH_3); ^{13}C NMR (150 MHz, CD_3OD): δ 177.3 (C-28), 144.0 (C-13), 138.1 (C-12), 128.2 (two), 124.1, 122.8, 121.1 (two), 104.0 (C-1′), 101.6 (Rha-1-C), 100.6 (Rha-1-C), 88.9, 79.0, 77.8, 76.7, 75.0, 72.5, 72.3, 71.0, 70.7, 70.6, 69.3, 68.6, 60.6, 55.9, 48.4, 46.9, 46.3, 41.6, 41.2, 39.3, 38.8, 38.6, 36.4, 33.7, 32.4, 32.2, 30.2, 27.2, 27.1, 25.8, 25.2, 23.2, 22.7 (two), 17.9, 16.6, 16.5, 16.4, 15.8, 14.6; HRMS (ESI) *m/z* calcd for $C_{54}H_{84}NO_{15}$ $[M+H]^+$ 986.5774, found 986.5776.

4.9.2. N-{3β-O-[2, 4-di-O-(a-L-rhamnopyranosyl)-β-D-glucopyranosyl]-olean-12-en-28-oyl}-2-methoxyaniline (**12b**)

Compound **12b** was obtained as a white solid in 94% yield; m. p.: 201.3—202.7 °C; ^{1}H NMR (600 MHz, CD_3OD): δ 8.26 (d, 1H, *J* = 8.0 Hz, Ar—H), 7.05 (t, 1H, *J* = 7.2 Hz, Ar—H), 6.99 (d, 1H, *J* = 7.9 Hz, Ar—H), 6.90 (t, 1H, *J* = 7.7 Hz, Ar—H), 5.54 (t-like, 1H, H-12), 5.36 (s, 1H, Rha-H-1), 4.42 (d, 1H, *J* = 7.7 Hz, H-1′), 3.90 (s, 3H, OCH_3), 3.80 (d, 1H, *J* = 11.1 Hz), 3.74 (dd, 1H, *J* = 9.5, 3.2 Hz, Rha-H-3), 3.66 (dd, 1H, *J* = 12.0, 3.8 Hz, H-6′-1), 3.63 (dd, 1H, *J* = 9.4, 3.1 Hz, Rha-H-3), 3.59 (t, 1H, *J* = 8.7 Hz), 3.54 (t, 1H, *J* = 9.1 Hz), 3.47—3.36 (m, 3H), 2.74 (d, 1H, *J* = 12.1 Hz, H-18), 1.27 (d, 3H, *J* = 6.1 Hz, Rha-H-6), 1.20 (d, 6H, *J* = 8.4 Hz, Rha-H-6, CH_3), 1.04, 0.96, 0.94, 0.89, 0.83, 0.62 (each s, each 3H, each CH_3); ^{13}C NMR (150 MHz, CD_3OD): δ 177.1 (C-28), 148.7, 143.4 (C-13), 127.2 (C-12), 123.9, 120.4, 119.5, 109.9, 104.0 (C-1′), 101.7 (Rha-C-1), 100.6 (Rha-C-1), 88.9, 79.0, 77.8, 76.7, 75.0, 72.5, 72.3, 71.0, 70.7, 70.6, 69.3, 68.6, 60.6, 55.8, 55.0, 47.6, 46.6, 46.5 (three), 42.3, 41.7, 39.3, 38.8, 38.7, 36.4, 33.7, 32.4, 32.2, 32.0, 30.2, 27.1, 27.0, 25.8, 25.0, 23.5, 23.3, 22.6, 17.8, 16.6, 16.5, 15.7, 15.6, 14.7; HRMS (ESI) *m/z* calcd for $C_{55}H_{86}NO_{16}$ $[M+H]^+$ 1016.5891, found 1016.5892.

4.9.3. N-{3β-O-[2, 4-di-O-(a-L-rhamnopyranosyl)-β-D-glucopyranosyl]-olean-12-en-28-oyl}-3-methoxyaniline (**12c**)

Compound **12c** was obtained as a white solid in 91% yield; m. p.: 176.2—178.2 °C; ^{1}H NMR (600 MHz, CD_3OD): δ 7.20 (t, 1H, *J* = 2.0 Hz, Ar—H), 7.18 (t, 1H, *J* = 8.2 Hz, Ar—H), 7.01—6.98 (m, 1H, Ar—H), 6.66 (dd, 1H, *J* = 8.3, 2.3 Hz, Ar—H), 5.44 (t-like, 1H, H-12), 5.36 (s, 1H, Rha-H-1), 4.42 (d, 1H, *J* = 7.7 Hz, H-1′), 3.91 (dd, 1H, *J* = 9.5, 6.3 Hz, Rha-H-4), 3.77 (s, 3H, OCH_3), 3.74 (dd, 1H, *J* = 9.6, 3.4 Hz, Rha-H-3), 3.66 (dd, 1H, *J* = 12.0, 3.9 Hz, H-6′-1), 3.63 (dd, 1H, *J* = 9.5, 3.3 Hz, Rha-H-3), 3.59 (t, 1H, *J* = 8.7 Hz), 3.54 (t, 1H, *J* = 9.0 Hz), 3.46—3.36 (m, 3H), 2.94 (dd, 1H, *J* = 13.2, 3.2 Hz, H-18), 1.26 (d, 3H, *J* = 6.2 Hz, Rha-H-6), 1.21 (d, 3H, *J* = 6.3 Hz, Rha-H-6), 1.20, 1.04, 0.98, 0.94, 0.92, 0.84, 0.74 (each s, each 3H, each CH_3); ^{13}C NMR (150 MHz, CD_3OD): δ 177.3 (C-28), 159.9, 144.0 (C-13), 139.3 (C-12), 128.99, 122.8, 113.1, 109.6, 106.8, 104.1 (C-1′), 101.6 (Rha-C-1), 100.6 (Rha-C-1), 88.9, 79.0, 77.8, 76.7, 75.0, 72.5, 72.3, 71.0, 70.7, 70.6, 69.3, 68.6, 60.6, 55.9, 54.3, 48.5, 46.9, 46.4 (two), 46.3, 41.6, 41.2, 39.3, 38.8, 38.6, 36.4, 33.8, 32.4, 32.3, 32.2, 30.2, 27.2, 27.1, 25.8, 25.2, 23.2, 22.7, 17.9, 16.6, 16.5, 16.4, 15.8, 14.7; HRMS (ESI) *m/z* calcd for $C_{55}H_{86}NO_{16}$ $[M+H]^+$ 1016.5859, found 1016.5854.

4.9.4. N-{3β-O-[2, 4-di-O-(a-L-rhamnopyranosyl)-β-D-glucopyranosyl]-olean-12-en-28-oyl}-4-methoxyaniline (**12d**)

Compound **12d** was obtained as a white solid in 91% yield; m. p.: 225.3—227.1 °C; ^{1}H NMR (600 MHz, CD_3OD): δ 7.33 (d, 2H, *J* = 9.0 Hz, Ar—H), 6.86 (d, 2H, *J* = 9.0 Hz, Ar—H), 5.43 (t-like, 1H, H-12), 5.36 (s, 1H, Rha-H), 4.42 (d, 1H, *J* = 7.7 Hz, H-1′), 3.91 (dd, 1H, *J* = 9.4, 6.2 Hz, Rha-H-4), 3.80 (d, 1H, *J* = 10.6 Hz), 3.76 (s, 3H, OCH_3), 3.66 (dd, 1H, *J* = 12.0, 4.0 Hz), 3.63 (dd, 1H, *J* = 9.4, 3.0 Hz, Rha-H-3), 3.59 (t, 1H, *J* = 8.7 Hz), 3.54 (t, 1H, *J* = 9.1 Hz), 3.46—3.36 (m, 3H), 3.15 (dd, 1H, *J* = 11.7, 4.2 Hz, H-3), 2.93 (dd, 1H, *J* = 13.0, 3.3 Hz, H-18), 1.26 (d, 3H, *J* = 6.2 Hz, Rha-H-6), 1.21 (d, 3H, *J* = 6.2 Hz, Rha-H-6), 1.20, 1.04, 0.98, 0.93, 0.92, 0.84, 0.76 (each s, each 3H, each CH_3); ^{13}C NMR (150 MHz, CD_3OD): δ 177.2 (C-28), 156.7, 144.0 (C-13), 131.0 (C-12), 123.0, 122.8 (two), 113.4 (two), 104.0 (C-1′), 101.6 (Rha-1-C), 100.6 (Rha-1-C), 88.9, 79.1, 77.8, 76.7, 75.0, 72.5, 72.3, 71.0, 70.7, 70.6, 69.4, 68.6, 60.6, 55.9, 54.5 (two), 53.4, 46.7, 46.3, 41.6, 41.2, 39.3, 38.8, 38.7, 36.5, 33.8, 32.5, 32.4, 32.2, 30.2, 27.2 (two), 25.8, 25.2, 23.2, 22.7, 17.9, 16.6, 16.5 (two), 15.8, 14.7, 7.8; HRMS (ESI) *m/z* calcd for $C_{55}H_{86}NO_{16}$ $[M+H]^+$ 1016.5870, found 1016.5870.

4.9.5. N-{3β-O-[2, 4-di-O-(a-L-rhamnopyranosyl)-β-D-glucopyranosyl]-olean-12-en-28-oyl}-2-chloroaniline (**12e**)

Compound **12e** was obtained as a white solid in 92% yield; m. p.: 239.1—240.7 °C; ^{1}H NMR (600 MHz, CD_3OD): δ 8.09 (d, 1H, *J* = 8.2 Hz, Ar—H), 7.43 (dd, 1H, *J* = 8.0, 1.2 Hz, Ar—H), 7.36—7.20 (m, 1H, Ar—H), 7.20—7.04 (m, 1H, Ar—H), 5.47 (t-like, 1H, H-12), 5.36 (s, 1H, Rha-H-1), 4.42 (d, 1H, *J* = 7.7 Hz, H-1′), 3.91 (dd, 1H, *J* = 9.5, 6.2 Hz, Rha-H-4), 3.84 (dd, 1H, *J* = 2.9, 1.7 Hz, Rha-H-2), 3.74 (dd, 1H, *J* = 9.5, 3.3 Hz, Rha-H-3), 3.66 (dd, 1H, *J* = 12.1, 3.9 Hz, H-6′-1), 3.63 (dd, 1H, *J* = 9.4, 3.3 Hz, Rha-H-3), 3.58 (t, 1H, *J* = 8.7 Hz), 3.54 (t, 1H, *J* = 9.0 Hz), 3.46—3.36 (m, 3H), 3.15 (dd, 1H, *J* = 11.7, 4.2 Hz, H-3), 2.85 (dd, 1H, *J* = 12.4, 2.8 Hz, H-18), 1.26 (d, 3H, *J* = 6.2 Hz, Rha-H-6), 1.20 (d, 3H, *J* = 6.3 Hz, Rha-H-6), 1.21, 1.04, 0.98, 0.95, 0.90, 0.84, 0.71 (each s, each 3H, each CH_3); ^{13}C NMR (150 MHz, CD_3OD): δ 177.2 (C-28), 143.3 (C-13), 134.6 (C-12), 129.0, 127.2, 125.3, 125.0, 124.0, 123.3, 104.0 (C-1′), 101.6 (Rha-1-C), 100.6 (Rha-1-C), 88.9, 79.0, 77.8, 76.7, 75.0, 72.5, 72.3, 71.0, 70.7, 70.6, 69.4, 68.6, 60.6, 55.8, 53.4, 47.6, 46.5, 46.4, 42.0, 41.6, 39.3, 38.8, 38.6, 36.4, 33.7, 32.6, 32.3, 32.0, 30.2, 27.1, 25.8, 25.2, 23.3, 23.2, 22.6, 17.8, 16.6, 16.5, 16.2, 15.7, 14.7, 7.9; HRMS (ESI) *m/z* calcd for $C_{54}H_{83}ClNO_{15}$ $[M+H]^+$ 1020.5378, found 1020.5389.

*4.9.6. N-{3β-O-[2, 4-di-O-(a-L-rhamnopyranosyl)-β-D-glucopyranosyl]-olean-12-en-28-oyl}-benzylamine (**12f**)*

Compound **12f** was obtained as a white solid in 90% yield; m. p.: 198.6–200.4 °C; ^{1}H NMR (600 MHz, CD_3OD): δ 7.70 (s, 1H, *J* = 5.8 Hz, N*H*CH_2), 7.30–7.27 (m, 4H, Ar–H), 7.25–7.20 (m, 1H, Ar–H), 5.37 (s, 1H, Rha-H-1), 5.32 (t-like, 1H, H-12), 4.85 (s, 1H, Rha-H-1), 4.42 (d, 1H, *J* = 7.7 Hz, H-1′), 4.38 (dd, 1H, *J* = 14.7, 5.9 Hz, NHC*H*$_2$-1), 4.27 (dd, 1H, *J* = 14.7, 5.7 Hz, NHC*H*$_2$-2), 4.01–3.95 (m, 2H), 3.94–3.88 (m, 1H), 3.85–3.83 (m, 1H, Rha-H-2), 3.80 (d, 1H, *J* = 10.6 Hz), 3.75 (dd, 1H, *J* = 9.6, 3.3 Hz, Rha-H-3), 3.66 (dd, 1H, *J* = 12.0, 3.9 Hz, H-6′-1), 3.63 (dd, 1H, *J* = 9.4, 3.2 Hz, Rha-H-3), 3.58 (t, 1H, *J* = 8.7 Hz), 3.54 (t, 1H, *J* = 9.1 Hz), 3.47–3.36 (m, 3H), 3.15 (dd, 1H, *J* = 11.7, 4.1 Hz, H-3), 2.82 (dd, 1H, *J* = 13.2, 3.5 Hz, H-18), 1.27 (d, 3H, *J* = 6.2 Hz, Rha-H-6), 1.22 (d, 3H, *J* = 6.2 Hz, Rha-H-6), 1.16, 1.05, 0.95, 0.91, 0.90, 0.86, 0.59 (each s, each 3H, each CH_3); ^{13}C NMR (150 MHz, CD_3OD): δ 179.9 (C-28), 179.8, 145.0 (C-13), 140.1, 129.2 (two), 128.6, 127.8, 123.8 (C-12), 105.2 (C-1′), 102.8 (Rha-C-1), 101.7 (Rha-C-1), 90.1, 80.2, 78.9, 77.9, 76.2, 73.7, 73.4, 72.2, 71.9, 71.7, 70.5, 69.7, 61.7, 57.0, 47.4, 47.3 (two), 44.2, 44.0, 42.7, 42.4 (two), 40.4, 40.0, 39.8, 37.6, 34.9, 34.1, 33.6, 33.3, 31.4, 28.3, 28.2, 26.9, 26.2, 24.3, 23.8, 19.0, 17.8, 17.7, 17.6, 16.9, 15.8; HRMS (ESI) *m/z* calcd for $C_{55}H_{86}NO_{15}$ $[M+H]^+$ 1000.5997, found 1000.5923.

*4.9.7. N-{3β-O-[2, 4-di-O-(a-L-rhamnopyranosyl)-β-D-glucopyranosyl]-olean-12-en-28-oyl}-2-pyridinemethanamine (**12g**)*

Compound **12g** was obtained as a white solid in 91% yield; m. p.: 198.0–199.2 °C; ^{1}H NMR (600 MHz, CD_3OD): δ 8.49 (d, 1H, *J* = 4.5 Hz, Ar–H), 7.80–7.76 (m, 1H, Ar–H), 7.36 (d, 1H, *J* = 7.9 Hz, Ar–H), 7.31–7.28 (m, 1H, Ar–H), 5.39 (t-like, 1H, H-12), 5.36 (s, 1H, Rha-H-1), 4.85 (s, 1H, Rha-H-1), 4.46 (d, 1H, *J* = 15.8 Hz, NHC*H*$_2$-1), 4.42 (d, 1H, *J* = 7.6 Hz, H-1′), 4.41 (d, 1H, *J* = 15.9 Hz, NHC*H*$_2$-2), 3.91 (dd, 1H, *J* = 9.5, 6.2 Hz, Rha-H-4), 3.84 (dd, 1H, *J* = 2.8, 1.8 Hz, Rha-H-2), 3.80 (d, 1H, *J* = 10.6 Hz), 3.75 (dd, 1H, *J* = 9.6, 3.4 Hz, Rha-H-3), 3.66 (dd, 1H, *J* = 12.1, 4.0 Hz, H-6′-1), 3.63 (dd, 1H, *J* = 9.5, 3.3 Hz, Rha-H-3), 3.60–3.56 (m, 1H), 3.54 (t, 1H, *J* = 9.1 Hz), 3.46–3.42 (m, 1H), 3.42–3.37 (m, 2H), 3.15 (dd, 1H, *J* = 11.7, 4.2 Hz, H-3), 2.82 (dd, 1H, *J* = 13.1, 3.5 Hz, H-18), 1.26 (d, 3H, *J* = 6.2 Hz, Rha-H-6), 1.21 (d, 3H, *J* = 6.2 Hz, Rha-H-6), 1.17, 1.04, 0.96, 0.92, 0.86, 0.84, 0.54 (each s, each 3H, each CH_3); ^{13}C NMR (150 MHz, CD_3OD): δ 178.9 (C-28), 157.4, 148.3, 143.6 (C-13), 137.3 (C-12), 123.0, 122.4, 122.0, 104.1 (C-1′), 101.6 (Rha-C-1), 100.6 (Rha-C-1), 88.9, 79.0, 77.8, 76.7, 75.0, 72.5, 72.3, 71.0, 70.7, 70.6, 69.4, 68.6, 60.6, 55.8, 46.3, 46.2, 44.1, 41.5, 39.2, 38.8, 38.6, 36.4, 33.7, 32.7, 32.4, 32.2, 30.2, 29.3 (two), 27.1 (two), 25.8, 25.1, 23.1, 22.8, 22.6, 17.8, 16.6, 16.5, 16.1, 15.8, 14.6, 7.8; HRMS (ESI) *m/z* calcd for $C_{54}H_{85}N_2O_{15}$ $[M+H]^+$ 1001.5950, found 1001.5924.

*4.9.8. N-{3β-O-[2, 4-di-O-(a-L-rhamnopyranosyl)-β-D-glucopyranosyl]-olean-12-en-28-oyl}-2-furyl-methylamin (**12h**)*

Compound **12h** was obtained as a white solid in 91% yield; m. p.: 214.8–215.9 °C; ^{1}H NMR (600 MHz, CD_3OD): δ 7.38 (d, 1H, *J* = 0.9 Hz, Furan-H), 6.32 (dd, 1H, *J* = 2.9, 1.9 Hz, Furan-H), 6.20 (d, 1H, *J* = 3.1 Hz, Furan-H), 5.36 (s, 1H, Rha-H-1), 5.32 (t-like, 1H, H-12), 4.42 (d, 1H, *J* = 7.7 Hz, H-1′), 4.34 (d, 1H, *J* = 15.4 Hz, NHC*H*$_2$-1), 4.28 (d, 1H, *J* = 15.4 Hz, NHC*H*$_2$-2), 3.91 (dd, 1H, *J* = 9.4, 6.2 Hz, Rha-H-4), 3.80 (d, 1H, *J* = 10.7 Hz), 3.75 (dd, 1H, *J* = 9.6, 3.3 Hz, Rha-H-3), 3.66 (dd, 1H, *J* = 12.1, 4.0 Hz, H-6′-1), 3.63 (dd, 1H, *J* = 9.5, 3.2 Hz, Rha-H-3), 3.58 (t, 1H, *J* = 8.7 Hz), 3.54 (t, 1H, *J* = 9.0 Hz), 3.47–3.36 (m, 3H), 3.15 (dd, 1H, *J* = 11.7, 4.1 Hz, H-3), 2.78 (dd, 1H, *J* = 13.1, 3.4 Hz, H-18), 1.26 (d, 3H, *J* = 6.2 Hz, Rha-H-6), 1.21 (d, 3H, *J* = 6.2 Hz, Rha-H-6), 1.15, 1.04, 0.94, 0.91, 0.91, 0.85, 0.61 (each s, each 3H, each CH_3); ^{13}C NMR (150 MHz, CD_3OD): δ 178.6 (C-28), 151.8, 143.8, 141.6 (C-13), 122.7 (C-12), 109.9, 106.8, 104.1 (C-1′), 101.5 (Rha-1-C), 100.6 (Rha-1-C), 89.0, 79.0, 77.8, 76.7, 75.0, 72.5, 72.3, 71.0, 70.7, 70.6, 69.3, 68.6, 60.6, 55.9, 46.3, 46.2, 41.5, 41.2, 39.2, 38.8, 38.7, 36.4, 35.9, 33.7, 32.7, 32.5, 32.2, 30.2, 27.1, 27.0, 25.8, 25.1, 23.2, 22.7, 22.6, 17.9, 16.6, 16.5, 16.1, 15.8, 14.7; HRMS (ESI) *m/z* calcd for $C_{53}H_{84}NO_{16}$ $[M+H]^+$ 990.5727, found 990.5743.

*4.9.9. N-{3β-O-[2, 4-di-O-(a-L-rhamnopyranosyl)-β-D-glucopyranosyl]-olean-12-en-28-oyl}-2-thiophenemethylamine (**12i**)*

Compound **12i** was obtained as a white solid in 94% yield; m. p.: 227.1–228.3 °C; ^{1}H NMR (600 MHz, CD_3OD): δ 7.25 (d, 1H, *J* = 5.1 Hz, Thiophene-H-5), 6.96 (d, 1H, *J* = 3.4 Hz, Thiophene-H-3), 6.91 (dd, 1H, *J* = 5.0, 3.5 Hz, Thiophene-H-4), 5.36 (s, 1H, Rha-H-1), 5.32 (t-like, 1H, H-12), 4.85 (d, 1H, *J* = 1.1 Hz, Rha-H-1), 4.54 (d, 1H, *J* = 15.1 Hz, NHC*H*$_2$-1), 4.44 (d, 1H, *J* = 14.9 Hz, NHC*H*$_2$-2), 4.42 (d, 1H, *J* = 7.7 Hz, H-1′), 3.91 (dd, 1H, *J* = 9.5, 6.2 Hz, Rha-H-4), 3.84 (dd, 1H, *J* = 2.7, 1.9 Hz, Rha-H-2), 3.79 (dd, *J* = 11.9, 1.4 Hz, 1H, H-6′-1), 3.74 (dd, 1H, *J* = 9.6, 3.4 Hz, Rha-H-3), 3.66 (dd, 1H, *J* = 12.1, 4.1 Hz, H-6′-2), 3.63 (dd, 1H, *J* = 9.5, 3.3 Hz, Rha-H-3), 3.58 (t, 1H, *J* = 8.7 Hz), 3.54 (t, 1H, *J* = 9.1 Hz), 3.46–3.37 (m, 3H), 3.15 (dd, 1H, *J* = 11.8, 4.2 Hz, H-3), 2.78 (dd, 1H, *J* = 13.1, 3.8 Hz, H-18), 1.26 (d, 3H, *J* = 6.2 Hz, Rha-H-6), 1.21 (d, 3H, *J* = 6.2 Hz, Rha-H-6), 1.15, 1.04, 0.94, 0.91, 0.90, 0.85, 0.61 (each s, each 3H, each CH_3); ^{13}C NMR (150 MHz, CD_3OD): δ 177.0 (C-28), 142.2 (C-13), 140.0 (C-12), 124.6, 124.0, 122.9, 121.2, 102.5 (C-1′), 100.1 (Rha-1-C), 99.1, 87.5, 77.6, 76.3, 75.2, 73.5, 71.0, 70.8, 69.5, 69.2, 69.1, 67.9, 67.1, 59.1, 54.4, 46.1, 44.8, 44.6, 40.0, 39.7, 37.7, 37.3, 37.1, 36.1, 34.9, 32.2, 31.2, 30.9, 30.6, 28.7, 27.8, 25.6 (two), 24.3, 23.5, 21.6, 21.2, 21.1, 16.4, 15.1, 15.0, 14.7, 14.3, 13.1; HRMS (ESI) *m/z* calcd for $C_{53}H_{84}NO_{15}S$ $[M+H]^+$ 1006.5562, found 1006.5507.

*4.9.10. N-methyl-N-{3β-O-[2, 4-di-O-(a-L-rhamnopyranosyl)-β-D-glucopyranosyl]-olean-12-en-28-oyl}-benzylamine (**12j**)*

Compound **12j** was obtained as a white solid in 91% yield; m. p.: 211.3–212.4 °C; ^{1}H NMR (600 MHz, CD_3OD): δ 7.35–7.28 (m, 2H, Ar–H), 7.28–7.19 (m, 3H, Ar–H), 5.37 (s, 1H, Rha-H-1), 5.21 (t-like, 1H, H-12), 4.43 (d, 1H, *J* = 7.7 Hz, H-1′), 4.01–3.96 (m, 2H), 3.94–3.88 (m, 1H), 3.84 (dd, 1H, *J* = 3.0, 1.7 Hz, Rha-H-2), 3.80 (d, 1H, *J* = 10.7 Hz), 3.76 (dd, 1H, *J* = 9.6, 3.3 Hz, Rha-H-3), 3.66 (dd, 1H, *J* = 13.9, 3.4 Hz), 3.63 (dd, 2H, *J* = 9.5, 3.1 Hz), 3.60–3.53 (m, 2H), 3.48–3.36 (m, 3H), 3.16 (dd, 1H, *J* = 11.7, 3.9 Hz, H-3), 3.06 (s, 3H, NC*H*$_3$), 1.27 (d, 3H, *J* = 6.2 Hz, Rha-H-6), 1.22 (d, 3H, *J* = 6.2 Hz, Rha-H-6), 1.17, 1.06, 0.97, 0.96, 0.92, 0.87, 0.78 (each s, each 3H, each CH_3); ^{13}C NMR (150 MHz, CD_3OD): δ 178.5 (C-28), 145.7 (C-13), 138.7, 130.3, 129.4 (two), 129.3, 128.3, 128.0, 127.1, 127.0, 122.9 (C-12), 105.2 (C-1′), 102.8 (Rha-C-1), 101.7 (Rha-C-1), 90.1, 80.2, 79.0, 77.9, 76.2, 73.7, 73.4, 72.2, 71.9 (two), 71.7, 70.5, 69.8, 61.7, 57.2, 54.4, 47.5, 42.9, 40.3, 40.0 (two), 39.8, 37.7 (two), 36.9, 34.7, 33.9, 33.3, 31.1 (two), 28.7, 28.3, 27.0, 26.4, 24.3, 19.1, 17.8, 17.7, 17.6, 16.9, 15.9; HRMS (ESI) *m/z* calcd for $C_{56}H_{88}NO_{15}$ $[M+H]^+$ 1014.6088, found 1014.6086.

*4.9.11. N-{3β-O-[2, 4-di-O-(a-L-rhamnopyranosyl)-β-D-glucopyranosyl]-olean-12-en-28-oyl}-2-fluorobenzylamine (**12k**)*

Compound **12k** was obtained as a white solid in 92% yield; m. p.: 245.1–246.3 °C; ^{1}H NMR (600 MHz, CD_3OD): δ 7.36–7.31 (m, 1H, Ar–H), 7.30–7.23 (m, 1H, Ar–H), 7.13–7.08 (m, 1H, Ar–H), 7.08–7.01 (m, 1H, Ar–H), 5.37 (s, 1H, Rha-H-1), 5.32 (t-like, 1H, H-12), 4.85 (s, 1H, Rha-H-1), 4.46–4.32 (m, 3H, H-1′, NHC*H*$_2$Ph), 3.91 (dd, 1H, *J* = 9.3, 6.2 Hz, Rha-H-4), 3.86–3.82 (m, 1H), 3.79 (d, 1H, *J* = 11.0 Hz), 3.75 (dd, 1H, *J* = 9.5, 3.2 Hz, Rha-H-3), 3.69–3.60 (m, 2H), 3.60–3.50 (m, 2H), 3.47–3.35 (m, 3H), 3.15 (dd, 1H, *J* = 11.5, 3.6 Hz, H-3), 2.80 (dd, 1H, *J* = 13.3, 2.7 Hz, H-18), 1.27 (d, 3H, *J* = 6.2 Hz, Rha-H-6), 1.21 (d, 3H, *J* = 6.1 Hz, Rha-H-6), 1.15, 1.04, 0.95, 0.91, 0.90, 0.85, 0.55 (each s, each 3H, each CH_3); ^{13}C NMR (150 MHz, CD_3OD): δ 180.0 (C-28), 163.2, 160.8, 144.9 (C-13), 130.9,

130.3, 129.9, 129.3, 127.1, 126.9, 124.9 (C-12), 116.0, 115.7, 105.2 (C-1′), 102.8 (Rha-C-1), 101.7 (Rha-C-1), 90.1, 80.1, 78.9, 77.9, 76.2, 73.7, 73.4, 72.2, 71.9, 71.7, 70.5, 69.7, 61.7, 57.0, 47.4, 42.6, 42.5, 40.3, 40.0, 39.8, 38.0, 37.6, 34.9, 34.0, 33.6, 33.3, 31.4, 30.5, 28.3, 26.9, 26.2, 24.3, 23.8, 19.0, 17.8, 17.7, 17.4, 16.9, 15.8; HRMS (ESI) *m/z* calcd for $C_{55}H_{85}FNO_{15}$ $[M+H]^+$ 1018.5842, found 1018.5842.

4.9.12. *N-{3β-O-[2, 4-di-O-(α-L-rhamnopyranosyl)-β-D-glucopyranosyl]-olean-12-en-28-oyl}-2-chlorobenzylamine (**12l**)*

Compound **12l** was obtained as a white solid in 89% yield; m. p.: 205.5–206.3 °C; ^{1}H NMR (600 MHz, CD_3OD): δ 7.61 (t-like, 1H, N*H*CH_2), 7.40–7.32 (m, 2H, Ar–H), 7.29–7.21 (m, 2H, Ar–H), 5.36 (s, 1H, Rha-H-1), 5.34 (t-like, 1H, H-12), 4.50–4.36 (m, 3H, H-1′, NHC*H*$_2$), 4.03–3.95 (m, 2H), 3.94–3.86 (m, 1H), 3.84 (s, 1H, Rha-H-2), 3.80 (d, 1H, J = 11.4 Hz, H-6′-1), 3.75 (dd, 1H, J = 9.6, 3.2 Hz, Rha-H-3), 3.70–3.60 (m, 2H), 3.60–3.53 (m, 2H), 3.44–3.40 (m, 3H), 3.15 (dd, 1H, J = 11.5, 3.8 Hz, H-3), 2.79 (dd, 1H, J = 13.3, 3.5 Hz, H-18), 1.27 (d, 3H, J = 6.2 Hz, Rha-H-6), 1.22 (d, 3H, J = 6.1 Hz, Rha-H-6), 1.16, 1.04, 0.96, 0.92, 0.90, 0.85, 0.54 (each s, each 3H, each CH_3); ^{13}C NMR (150 MHz, CD_3OD): δ 180.0 (C-28), 144.9 (C-13), 137.0, 134.3, 130.7, 130.2, 129.5, 127.8, 124.0 (C-12), 105.24 (C-1′), 102.9 (Rha-C-1), 101.7 (Rha-C-1), 90.1, 80.2, 79.0, 77.9, 76.2, 73.7, 73.5, 72.2, 71.9, 71.7, 70.5, 69.7, 64.9, 61.8, 57.0, 47.5 (two), 42.7 (two), 42.2, 40.4 (two), 40.0 (two), 37.6 (two), 34.9, 34.0, 33.6, 33.3, 31.4, 28.3, 26.9, 26.2, 24.3, 23.9, 23.8, 19.0, 17.8, 17.7, 17.4, 16.9, 15.8; HRMS (ESI) *m/z* calcd for $C_{55}H_{85}ClNO_{15}$ $[M+H]^+$ 1034.5509, found 1034.5516.

4.9.13. *N-{3β-O-[2, 4-di-O-(α-L-rhamnopyranosyl)-β-D-glucopyranosyl]-olean-12-en-28-oyl}-2-bromobenzylamine (**12m**)*

Compound **12m** was obtained as a white solid in 90% yield; m. p.: 175.4–176.3 °C; ^{1}H NMR (600 MHz, CD_3OD): δ 7.62–7.52 (m, 2H, Ar–H), 7.39–7.27 (m, 3H, Ar–H), 7.17 (t, 1H, J = 7.4 Hz, N*H*CH_2), 5.39–5.30 (m, 2H, Rha-H-1, H-12), 4.48–4.35 (m, 3H, H-1′, NHC*H*$_2$), 4.01–3.94 (m, 2H), 3.94–3.86 (m, 1H), 3.86–3.83 (m, 1H, Rha-H-2), 3.80 (d, 1H, J = 11.4 Hz, H-6′-1), 3.75 (dd, 1H, J = 9.5, 3.0 Hz, Rha-H-3), 3.70–3.60 (m, 2H), 3.60–3.50 (m, 2H), 3.48–3.36 (m, 3H), 3.15 (dd, 1H, J = 11.5, 3.6 Hz, H-3), 2.78 (dd, 1H, J = 12.6, 3.0 Hz, H-18), 1.27 (d, 3H, J = 6.1 Hz, Rha-H-6), 1.22 (d, 3H, J = 6.2 Hz, Rha-H-6), 1.16, 1.05, 0.96, 0.92, 0.90, 0.85, 0.55 (each s, each 3H, each CH_3); ^{13}C NMR (150 MHz, CD_3OD): δ 180.0 (C-28), 144.9 (C-13), 138.6, 133.5, 130.8, 129.8, 128.4, 124.2 (C-12), 124.1, 107.4, 105.2 (C-1′), 102.8 (Rha-C-1), 101.7 (Rha-C-1), 90.1, 80.2, 79.0, 77.9, 76.2, 73.7, 73.4, 72.2, 71.9 (two), 71.7, 70.5, 69.7, 61.7, 57.0, 47.5, 47.4, 44.6, 42.7 (two), 40.4, 40.0, 39.8, 37.6, 34.9, 34.0, 33.6, 33.3, 31.4 (two), 28.3, 26.9, 26.2, 24.3, 23.9, 23.8, 19.0, 17.8, 17.7, 17.4, 16.9, 15.8; HRMS (ESI) *m/z* calcd for $C_{55}H_{85}BrNO_{15}$ $[M+H]^+$ 1078.5037, found 1078.5027.

4.9.14. *N-{3β-O-[2, 4-di-O-(α-L-rhamnopyranosyl)-β-D-glucopyranosyl]-olean-12-en-28-oyl}-2-methoxybenzylamine (**12n**)*

Compound **12n** was obtained as a white solid in 89% yield; m. p.: 174.9–175.8 °C; ^{1}H NMR (600 MHz, CD_3OD): δ 7.25 (t, 2H, J = 6.1 Hz, Ar–H), 7.19 (d, 1H, J = 7.0 Hz, Ar–H), 6.95 (d, 1H, J = 8.3 Hz, Ar–H), 6.88 (t-like, 1H, N*H*CH_2), 5.36 (s, 1H, Rha-H-1), 5.31 (t-like, 1H, H-12), 4.42 (d, 1H, J = 7.6 Hz, H-1′), 4.35 (d, 2H, J = 5.3 Hz, NHC*H*$_2$), 4.00–3.95 (m, 2H), 3.94–3.90 (m, 1H), 3.88 (s, 3H, OCH_3), 3.84 (s, 1H, Rha-H-2), 3.80 (d, 1H, J = 11.6 Hz), 3.75 (dd, 1H, J = 9.6, 3.1 Hz, Rha-H-3), 3.69–3.60 (m, 2H), 3.59–3.53 (m, 2H), 3.47–3.36 (m, 3H), 3.14 (dd, 1H, J = 11.3, 3.7 Hz, H-3), 2.67 (dd, 1H, J = 12.9, 2.5 Hz, H-18), 1.27 (d, 3H, J = 6.4 Hz, Rha-H-6), 1.22 (d, 3H, J = 5.8 Hz, Rha-H-6), 1.04, 0.94, 0.91, 0.87, 0.85, 0.46 (each s, each 3H, each CH_3); ^{13}C NMR (150 MHz, CD_3OD): δ 179.5 (C-28), 158.7, 145.1 (C-13), 130.1, 129.6, 127.1, 123.8 (C-12), 121.3, 111.1, 105.2 (C-1′), 102.8 (Rha-C-1), 101.7 (Rha-C-1), 90.1, 80.1, 78.9, 77.8, 76.2, 73.6, 73.5, 72.1, 71.8, 71.7, 70.5, 69.7, 61.7, 61.3, 57.0, 55.6, 47.6, 47.5, 47.4, 42.9, 42.7, 40.3, 40.1, 40.0, 39.8, 37.5, 34.9, 33.8, 33.3, 31.3, 28.3, 28.1, 26.9, 26.2, 24.3, 24.0, 23.7, 19.0, 17.8, 17.7, 17.2, 16.9, 15.9, 9.2; HRMS (ESI) *m/z* calcd for $C_{56}H_{88}NO_{16}$ $[M+H]^+$ 1030.6031, found 1030.6031.

4.9.15. *N-{3β-O-[2, 4-di-O-(α-L-rhamnopyranosyl)-β-D-glucopyranosyl]-olean-12-en-28-oyl}-2-phenylethylamine (**12o**)*

Compound **12o** was obtained as a white solid in 93% yield; m. p.: 199.6–200.7 °C; ^{1}H NMR (600 MHz, CD_3OD): δ 7.34–7.26 (m, 2H, Ar–H), 7.26–7.18 (m, 3H, Ar–H), 6.94–6.87 (t-like, 1H, N*H*CH_2), 5.36 (s, 1H, Rha-H-1), 5.13 (t-like, 1H, H-12), 4.42 (d, 1H, J = 7.7 Hz, H-1′), 4.02–3.95 (m, 2H), 3.95–3.86 (m, 1H), 3.86–3.82 (m, 1H, Rha-H-2), 3.82–3.77 (m, 1H, H-6-1′), 3.74 (dd, 1H, J = 9.5, 3.1 Hz, Rha-H-3), 3.70–3.60 (m, 2H), 3.60–3.53 (m, 2H), 3.48–3.35 (m, 3H), 3.26–3.18 (m, 1H, NHCH_2CH_2), 3.15 (dd, 1H, J = 11.7, 3.8 Hz, H-3), 2.88–2.69 (m, 3H, NHCH_2CH_2), 2.59 (dd, 1H, J = 12.6, 3.6 Hz, H-18), 1.27 (d, 3H, J = 6.2 Hz, Rha-H-6), 1.21 (d, 3H, J = 6.2 Hz, Rha-H-6), 1.13, 1.04, 0.92, 0.91, 0.90, 0.86, 0.65 (each s, each 3H, each CH_3); ^{13}C NMR (150 MHz, CD_3OD): δ 180.1 (C-28), 144.9 (C-13), 140.3, 129.7 (two), 129.4 (two), 127.3 (C-12), 105.2 (C-1′), 102.8 (Rha-C-1), 101.8 (Rha-C-1), 90.1, 80.2, 79.0, 77.9, 76.2, 73.7, 73.4, 72.2, 71.9, 71.7, 70.5, 69.8, 61.7, 57.0, 47.5, 47.3, 42.6, 42.5, 41.8, 40.4 (two), 40.0, 39.8, 37.6 (two), 36.1, 34.9, 33.7, 33.4, 33.3, 31.3 (two), 28.3, 28.2, 26.9, 26.2, 24.3, 24.0, 23.7, 19.0, 17.8, 17.7, 17.5, 16.9, 15.8; HRMS (ESI) *m/z* calcd for $C_{56}H_{88}NO_{15}$ $[M+H]^+$ 1014.6089, found 1014.6089.

4.9.16. *N-{3β-O-[2, 4-di-O-(α-L-rhamnopyranosyl)-β-D-glucopyranosyl]-olean-12-en-28-oyl}-3-phenylpropanamine (**12p**)*

Compound **12p** was obtained as a white solid in 92% yield; m. p.: 203.4–204.2 °C; ^{1}H NMR (600 MHz, CD_3OD): δ 7.28–7.22 (m, 2H, Ar–H), 7.20–7.12 (m, 3H, Ar–H), 5.37 (s, 1H, Rha-H-1), 5.34 (t-like, 1H, H-12), 4.42 (d, 1H, J = 7.6 Hz, H-1′), 4.00–3.95 (m, 2H), 3.95–3.86 (m, 1H), 3.86–3.83 (m, 1H, Rha-H-2), 3.80 (d, 1H, J = 11.6 Hz, H-6′-1), 3.75 (dd, 1H, J = 9.6, 3.2 Hz, Rha-H-3), 3.69–3.60 (m, 2H), 3.56 (dd, 2H, J = 11.2, 9.0 Hz), 3.48–3.34 (m, 3H), 3.27–3.20 (m, 1H), 3.15 (dd, 1H, J = 11.5, 3.8 Hz, H-3), 3.12–3.05 (m, 1H), 2.76 (dd, 1H, J = 12.7, 2.5 Hz, H-18), 2.66–2.59 (m, 2H), 1.27 (d, 3H, J = 6.2 Hz, Rha-H-6), 1.22 (d, 3H, J = 6.1 Hz, Rha-H-6), 1.16, 1.05, 0.95, 0.92, 0.91, 0.86, 0.75 (each s, each 3H, each CH_3); ^{13}C NMR (150 MHz, CD_3OD): δ 180.0 (C-28), 179.9, 145.1 (C-13), 142.8, 129.2 (two), 129.1 (two), 126.7, 123.7 (C-12), 105.2 (C-1′), 102.8 (Rha-C-1), 101.7 (Rha-C-1), 90.1, 80.2, 78.9, 77.9, 76.2, 73.7, 73.4, 72.2 (two), 71.9, 71.7, 70.5, 69.7, 61.7, 57.0, 47.4, 47.2, 42.7, 42.4, 40.4, 40.3, 40.2, 40.0, 39.8, 37.6, 34.9, 34.2, 34.1, 33.6, 33.3, 31.9, 31.4, 28.3, 26.9, 26.3, 24.3, 23.8, 19.0, 17.8, 17.7 (two), 17.7, 16.9, 15.8; HRMS (ESI) *m/z* calcd for $C_{57}H_{90}NO_{15}$ $[M+H]^+$ 1028.6249, found 1028.6249.

4.10. *Pseudotyped SARS-CoV-2 infection assay*

HEK293T cells were seeded in 6 plate wells at 4 × 10^5/mL and cultured overnight. Pseudovirus (PsV) were produced by co-transfection HEK293T cells with pNL4-3.Luc.R-E− and plasmids encoding either SARS-CoV-2 S, or VSV-G by using Polyjet (SignaGen, USA). After 48 h of transfection, supernatants containing PsV were collected and cleared by 0.45 μM filtrations [23]. 293T-ACE2 cells were seeded (20,000 cells per well) in 96 wells plates. After 24 h, a mixture that was consisted of 50 μL gradient concentrations of compounds and 50 μL PsV supernatant was added to each well and incubated with cells for 48 h. Cells were lysed and luciferase activities were quantified by Luciferase assay system (Promega, USA).

4.11. *Cytotoxicity assay*

The cytotoxicity effect of the compounds on 293T-ACE2 or Vero-

E6 cells were measured by Methyl Thiazolyl Tetrazolium (MTT) assay [13,28]. In brief, monolayers cells in 96-well plates were rinsed by PBS and incubated with indicated compounds for 48 h subsequently. Then, cells were treated with 0.5 mg/mL MTT for 4 h at 37 °C and formazan crystals in viable cells were dissolved in 150 μL DMSO. The absorbance of solubilized formazan was measured by Synergy multimode reader (BioTek, American) at 570 nm.

4.12. Indirect immunofluorescence assay (IFA)

After the authentic SARS-CoV-2 inhibition assay, we fixed the cells with 4% paraformaldehyde (Bio-Rad) and permeabilized by using Triton X-100 (Sigma, USA). Cells were stained with polyclonal rabbit anti-NP antibody and a secondary peroxidase-labeled goat anti-rabbit IgG H&L (Alexa Fluor® 488) (Abcam). DAPI was used to color nucleus and images were acquired by Axio Observer microscope (Zeiss, Germany) [40] and chloroquine (CQ) was used as a positive control [23].

4.13. Authentic SARS-CoV-2 inhibition assay

Authentic SARS-CoV-2 inhibition assay was performed by Wuhan Institute of Virology, Chinese Academy of Sciences, as described previously [13,23]. Briefly, SARS-CoV-2 (Wuhan-HU-1) was incubated with different concentrations of compound **12f** for 1 h before placing the mixture on vero-E6 cells for another 1 h incubation (MOI = 0.01). After that, fresh medium with variant concentrations of **12f** was added and viral total RNA were extracted by Viral RNA/DNA Extraction Kit (Takara, Japan) after 24 h, and the S gene copies were quantified on ABI 7500 (Takara TB Green® Premix Ex Taq™ II, Japan) by using the primers reported before [23], *Foward*: GCTCCCTCTCATCAGTTCCA; *Reverse*: CTCAAGTG TCTGTGGATCACG.

4.14. Co-immunoprecipitation (Co-IP) assay and western blotting

Plasmids pcDNA3.1-ACE2-Flag and pcDNA3.1-SARS-S were co-transfected into 293T cells. Total protein was extracted after 48 h and then incubated with protein A Sepharose in conjunction with anti-flag antibody or mouse IgG. The samples were incubated overnight and separated by 10% PAGE subsequently, followed by transfer to nitrocellulose membranes (Roche, Germany). ACE2 and SARS-S were detected by anti-Flag (Sigma, USA) and anti-SARS-CoV-S (Sinol biological Inc., China) with mouse anti-goat-horseradish peroxidase (HRP) (Fude biological Technology Co., LTD., China) as the secondary antibody, respectively [41].

4.15. Surface plasmon resonance (SPR) measurement

Compound **12f** was fixed on the chip by photo-crosslinking, then recombinant SARS-CoV-2 S-trimer, S1 subunit or S2 subunit protein (DRA 47, DRA 48, DRA 49, Novoprotein Inc. Shanghai) at indicated concentrations were injected sequentially into the chamber in buffer PBST (0.1% Tween 20, pH 7.4), the interaction of S-trimer, S1 subunit or S2 subunit with **12f** fixed was detected by PlexArrayTM HT SPRi (Seattle, US). The reaction temperature was controlled at 4 °C, binding time was 600 s, disassociation time was 360 s, flow rate was 0.5 μL/s, the chip was regenerated with Glycine Hydrochloride (pH 2.0). The data of interaction signals was retrieved and analyzed with PlexeraDE software [42].

4.16. Cell-cell fusion assays

HEK-293T cells were transfected with pAAV-IRES-GFP-SARS-CoV-2 S or vehicle plasmid pAAV-IRES-GFP to construct effector cells by using Polyjet (SignaGen, USA) [13,23]. Targeted cells (Vero-E6) were seeded in 96 well plates (20,000 cells per well) 6 h prior to cell-cell fusion. Effector cells were firstly treated with different concentrations of compounds for 30 min, then were overlaid on targeted cells. After 24 h, three random fields were imaged by inverted fluorescence microscope (Zeiss, Germany) [13].

Declaration of competing interest

The authors declare that they have no known competing financial interests or personal relationships that could have appeared to influence the work reported in this paper.

Acknowledgments

This project was supported by the National Natural Science Foundation of China (82073722, 31872521); the Natural Science Foundation of Guangdong Province, China (2018A030313414); Major scientific and technological projects of Guangdong Province (2019B020202002); Science &Technology Project of Guangzhou, China (201804010457, 2020B111110001) and the special Project for prevention and control of SARS-CoV-2 from Educational Commission of Guangdong Province of China (2020KZDZX1039).

Appendix A. Supplementary data

Supplementary data to this article can be found online at https://doi.org/10.1016/j.ejmech.2021.113242.

References

[1] G. Nittari, G. Pallotta, F. Amenta, S.K. Tayebati, Current pharmacological treatments for SARS-COV-2: a narrative review, Eur. J. Pharmacol. 882 (2020) 173328.
[2] L.S. Wang, Y.R. Wang, D.W. Ye, Q.Q. Liu, Review of the 2019 novel coronavirus (SARS-CoV-2) based on current evidence, Int. J. Antimicrob. Agents 55 (2020) 105948.
[3] L. Wang, B.B. Bao, G.Q. Song, C. Chen, X.M. Zhang, W. Lu, Z.F. Wang, Y. Cai, S. Li, S. Fu, F.H. Song, H.T. Yang, J.G. Wang, Discovery of unsymmetrical aromatic disulfides as novel inhibitors of SARS-CoV main protease: chemical synthesis, biological evaluation, molecular docking and 3D-QSAR study, Eur. J. Med. Chem. 137 (2017) 450–461.
[4] R.J. Wu, K.X. Zhou, H.J. Yang, G.Q. Song, Y.H. Li, J.X. Fu, X. Zhang, S.J. Yu, L.Z. Wang, L.X. Xiong, C.W. Niu, F.H. Song, H.T. Yang, J.G. Wang, Chemical synthesis, crystal structure, versatile evaluation of their biological activities and molecular simulations of novel pyrithiobac derivatives, Eur. J. Med. Chem. 167 (2019) 472–484.
[5] H.A. Rothan, S.N. Byrareddy, The epidemiology and pathogenesis of coronavirus disease (COVID-19) outbreak, J. Autoimmun. 109 (2020) 102433.
[6] S.P. Adhikari, S. Meng, Y.J. Wu, Y.P. Mao, R.X. Ye, Q.Z. Wang, C. Sun, S. Sylvia, S. Rozelle, H. Raat, H. Zhou, Epidemiology, causes, clinical manifestation and diagnosis, prevention and control of coronavirus disease (COVID-19) during the early outbreak period: a scoping review, Infect. Dis. Poverty 9 (2020) 29.
[7] W.E. Wang, J.M. Tang, F.Q. Wei, Updated understanding of the outbreak of 2019 novel coronavirus (2019-nCoV) in Wuhan, China, J. Med. Virol. 92 (2020) 441–447.
[8] Coronavirus disease (COVID-19) weekly epidemiological update and weekly operational update. https://www.who.int/emergencies/diseases/novel-coronavirus-2019/situation-reports/, 2020.
[9] F. Krammer, SARS-CoV-2 vaccines in development, Nature 586 (2020) 516–527.
[10] A. Awadasseid, Y.L. Wu, Y. Tanaka, W. Zhang, Current advances in the development of SARS-CoV-2 vaccines, Int. J. Biol. Sci. 17 (2021) 8–19.
[11] M.L. Wang, R.Y. Cao, L.K. Zhang, X.L. Yang, J. Liu, M.Y. Xu, Z.L. Shi, Z.H. Hu, W. Zhong, G.F. Xiao, Remdesivir and chloroquine effectively inhibit the recently emerged novel coronavirus (2019-nCoV) in vitro, Cell Res. 30 (2020) 269–271.
[12] J.D. Monpara, S.J. Sodha, P.K. Gupta, COVID-19 associated complications and potential therapeutic targets, Eur. J. Pharmacol. 886 (2020) 173548.
[13] S. Xia, M.Q. Liu, C. Wang, W. Xu, Q.S. Lan, S.L. Feng, F.F. Qi, L.L. Bao, L.Y. Du, S.W. Liu, C. Qin, F. Sun, Z.L. Shi, Y. Zhu, S.B. Jiang, L. Lu, Inhibition of SARS-CoV-2 (previously 2019-nCoV) infection by a highly potent pan-coronavirus fusion inhibitor targeting its spike protein that harbors a high capacity to mediate membrane fusion, Cell Res. 30 (2020) 343–355.

[14] S.Y. Xiu, A. Dick, H. Ju, S. Mirzaie, F. Abdi, S. Cocklin, P. Zhan, X.Y. Liu, Inhibitors of SARS-CoV-2 entry: current and future opportunities, J. Med. Chem. 63 (2020) 12256–12274.
[15] I. Mercurio, V. Tragni, F. Busto, A.D. Grassi, C.L. Pierri, Protein structure analysis of the interactions between SARS-CoV-2 spike protein and the human ACE2 receptor: from conformational changes to novel neutralizing antibodies, Cell. Mol. Life Sci. (2020) 1–22.
[16] T. Tang, M. Bidon, J.A. Jaimes, G.R. Whittaker, S. Daniel, Coronavirus membrane fusion mechanism offers a potential target for antiviral development, Antivir. Res. 178 (2020) 104792.
[17] M. Hoffmann, H. Kleine-Weber, S. Schroeder, N. Krüger, T. Herrler, S. Erichsen, T.S. Schiergens, G. Herrler, N.H. Wu, A. Nitsche, M.A. Müller, C. Drosten, S. Pöhlmann, SARS-CoV-2 cell entry depends on ACE2 and TMPRSS2 and is blocked by a clinically proven protease inhibitor, Cell 181 (2020) 271–280.
[18] T.M. Clausen, D.R. Sandoval, C.B. Spliid, J. Pihl, H.R. Perrett, C.D. Painter, A. Narayanan, S.A. Majowicz, E.M. Kwong, R.N. McVicar, B.E. Thacker, C.A. Glass, Z. Yang, J.L. Torres, G.J. Golden, P.L. Bartels, R.N. Porell, A.F. Garretson, L. Laubach, J. Feldman, X. Yin, Y. Pu, B.M. Hauser, T.M. Caradonna, B.P. Kellman, C. Martino, P.L.S.M. Gordts, S.K. Chanda, A.G. Schmidt, K. Godula, S.L. Leibel, J. Jose, K.D. Corbett, A.B. Ward, A.F. Carlin, J.D. Esko, SARS-CoV-2 infection depends on cellular heparan sulfate and ACE2, Cell 183 (2020) 1043–1057.
[19] B. Ju, Q. Zhang, J.W. Ge, R.K. Wang, J. Sun, X.Y. Ge, J.Z. Yu, S.S. Shan, B. Zhou, S. Song, X. Tang, J.F. Yu, J. Lan, J. Yuan, H.Y. Wang, J.J. Zhao, S.Y. Zhang, Y.C. Wang, X.L. Shi, L. Liu, J.C. Zhao, X.Q. Wang, Z. Zhang, L.Q. Zhang, Human neutralizing antibodies elicited by SARS-CoV-2 infection, Nature 584 (2020) 115–119.
[20] M.A. Tortorici, M. Beltramello, F.A. Lempp, D. Pinto, H.V. Dang, L.E. Rosen, M. McCallum, J. Bowen, A. Minola, S. Jaconi, F. Zatta, A.D. Marco, B. Guarino, S. Bianchi, E.J. Lauron, H. Tucker, J.Y. Zhou, A. Peter, C. Havenar-Daughton, J.A. Wojcechowskyj, J.B. Case, R.E. Chen, H. Kaiser, M. Montiel-Ruiz, M. Meury, N. Czudnochowski, R. Spreafico, J. Dillen, C. Ng, N. Sprugasci, K. Culap, F. Benigni, R. Abdelnabi, S.C. Foo, M.A. Schmid, E. Cameroni, A. Riva, A. Gabrieli, M. Galli, M.S. Pizzuto, J. Neyts, M.S. Diamond, H.W. Virgin, G. Snell, D. Corti, K. Fink, D. Veesler, Ultrapotent human antibodies protect against SARS-CoV-2 challenge via multiple mechanisms, Science 370 (2020) 950–957.
[21] S. Du, Y.L. Cao, Q.Y. Zhu, P. Yu, F.F. Qi, G.P. Wang, X.X. Du, L.L. Bao, W. Deng, H. Zhu, J.N. Liu, J.H. Nie, Y.H. Zheng, H.Y. Liang, R.X. Liu, S.R. Gong, H. Xu, A. Yisimayi, Q. Lv, B. Wang, R.S. He, Y.L. Han, W.J. Zhao, Y.L. Bai, Y.J. Qu, X. Gao, C.G. Ji, Q. Wang, N. Gao, W. Huang, Y. Wang, X.S. Xie, X.D. Su, J.Y. Xiao, C. Qin, Structurally resolved SARS-CoV-2 antibody shows high efficacy in severely infected hamsters and provides a potent cocktail pairing strategy, Cell 183 (2020) 1013–1023.
[22] S.P. Yu, Y.Y. Zhu, J.R. Xu, G.T. Yao, P. Zhang, M.G. Wang, Y.F. Zhao, G.Q. Lin, H.Z. Chen, L.L. Chen, J.G. Zhang, Glycyrrhizic Acid Exerts Inhibitory Activity against the Spike Protein of SARS-CoV-2, Phytomedicine, 2020, https://doi.org/10.1016/j.phymed.2020.153364.
[23] C. Yang, X.Y. Pan, X.F. Xu, C. Cheng, Y. Huang, L. Li, S.B. Jiang, W. Xu, G.F. Xiao, S.W. Liu, Salvianolic acid C potently inhibits SARS-CoV-2 infection by blocking the formation of six-helix bundle core of spike protein, Signal Transduct. Target. Ther. 5 (2020) 22.
[24] C.E. Mair, U. Grienke, A. Wilhelm, E. Urban, M. Zehl, M. Schmidtke, J.M. Rollinger, Anti-influenza triterpene saponins from the bark of burkea Africana, J. Nat. Prod. 81 (2018) 515–523.
[25] F. Yu, Y.Y. Peng, Q. Wang, Y.Y. Shi, L.L. Si, H. Wang, Y.X. Zheng, E. Lee, S.L. Xiao, M.R. Yu, Development of bivalent oleanane-type triterpenes as potent HCV entry inhibitors, Eur. J. Med. Chem. 77 (2014) 258–268.
[26] L.L. Si, K. Meng, Z.Y. Tian, J.Q. Sun, H.Q. Li, Z.W. Zhang, V. Soloveva, H.W. Li, G. Fu, Q. Xia, S.L. Xiao, L.H. Zhang, D.M. Zhou, Triterpenoids manipulate a broad range of virus-host fusion via wrapping the HR2 domain prevalent in viral envelopes, Sci. Adv. 4 (2018), eaau8408.
[27] S.M. Li, X.H. Jia, X.T. Shen, Z.W. Wei, Z.Y. Jiang, Y.X. Liao, Y.M. Guo, X.J. Zheng, G.H. Zhong, G.P. Song, Structure-activity relationships of 3-O-β-chacotriosyl oleanic acid derivatives as entry inhibitors for highly pathogenic H5N1 influenza virus, Bioorg. Med. Chem. 25 (2017) 4384–4396.
[28] G.P. Song, X.T. Shen, S.M. Li, Y.B. Li, H.Z. Si, J.H. Fan, J.H. Li, E.Q. Gao, S.W. Liu, Structure-activity relationships of 3-O-β-chacotriosyl oleanane-type triterpenoids as potential H5N1 entry inhibitors, Eur. J. Med. Chem. 119 (2016) 109–121.
[29] M. Yu, L. Si, Y. Wang, Y. Wu, F. Yu, P. Jiao, Y. Shi, H. Wang, S. Xiao, G. Fu, K. Tian, Y. Wang, Z. Guo, X. Ye, L. Zhang, D. Zhou, Discovery of pentacyclic triterpenoids as potential entry inhibitors of influenza viruses, J. Med. Chem. 57 (2014) 10058–10071.
[30] J.M. White, S.E. Delos, M. Brecher, K. Schornberg, Structures and mechanisms of viral membrane fusion proteins: multiple variations on a common theme, Crit. Rev. Biochem. Mol. Biol. 43 (2008) 189–219.
[31] L. Cooper, A. Schafer, Y.F. Li, H. Cheng, B.M. Fagla, Z.N. Shen, R. Nowar, K. Dye, M. Anantpadma, R.A. Davey, G.R.J. Thatcher, L.J. Rong, R. Xiong, Screening and reverse-engineering of estrogen receptor ligands as potent pan-filovirus inhibitors, J. Med. Chem. 63 (2020) 11085–11099.
[32] G.P. Song, X.T. Shen, S.M. Li, H.Z. Si, Y.B. Li, H.Y. Luan, J.H. Fan, Q.Q. Liang, S.W. Liu, Discovery of 3-O-β-chacotriosyl oleanane-type triterpenes as H5N1 entry inhibitors, RSC Adv. 5 (2015) 39145–39154.
[33] A. Basu, D.M. Mills, D. Mitchell, E. Ndungo, J.D. Williams, A.S. Herbert, J.M. Dye, D.T. Moir, K. Chandran, J.L. Patterson, L. Rong, T.L. Bowlin, Novel small molecule entry inhibitors of Ebola virus, J. Infect. Dis. 212 (2015) S425–S434.
[34] G.P. Song, X.T. Shen, S.M. Li, Y.B. Li, Y.P. Liu, Y.S. Zheng, R.H. Lin, J.H. Fan, H.M. Ye, S.W. Liu, Structure-activity relationships of 3-O-β-chacotriosyl ursolic acid derivatives as novel H5N1 entry inhibitors, Eur. J. Med. Chem. 93 (2015) 431–442.
[35] J. Wang, H. Cheng, K. Ratia, E. Varhegyi, W.G. Hendrickson, J. Li, L. Rong, A comparative high-throughput screening protocol to identify entry inhibitors of enveloped viruses, J. Biomol. Screen 19 (2014) 100–107.
[36] I.N. Gaisina, N.P. Peet, L. Wong, A.M. Schafer, H. Cheng, M. Anantpadma, R.A. Davey, G.R.J. Thatcher, L. Rong, Discovery and structural optimization of 4-(aminomethyl)benzamides as potent entry inhibitors of Ebola and Marburg virus infections, J. Med. Chem. 63 (2020) 7211–7225.
[37] H. Cheng, C.M. Lear-Rooney, L. Johansen, E. Varhegyi, Z.W. Chen, G.G. Olinger, L. Rong, Inhibition of Ebola and Marburg virus entry by G protein-coupled receptor antagonists, J. Virol. 89 (2015) 9932–9938.
[38] G.P. Song, S. Yang, W. Zhang, Y.L. Cao, P. Wang, N. Ding, Z.H. Zhang, Y. Guo, Y.X. Li, Discovery of the first series of small molecule H5N1 entry inhibitors, J. Med. Chem. 52 (2009) 7368–7371.
[39] S.W. Liu, G.F. Xiao, Y.B. Chen, Y.X. He, J.K. Niu, C.R. Escalante, H.B. Xiong, J. Farmer, A.K. Debnath, P. Tien, Interaction between heptad repeat 1 and 2 regions in spike protein of SARS-associated coronavirus: implications for virus fusogenic mechanism and identification of fusion inhibitors, Lancet 363 (2004) 938–947.
[40] N. Kohmer, S. Westhaus, C. Rühl, S. Ciesek, H.F. Rabenau, Clinical performance of different SARS-CoV-2 IgG antibody tests, J. Med. Virol. 92 (2020) 2243–2247.
[41] C. Li, H. Chu, X.J. Liu, M.C. Chiu, X.Y. Zhao, D. Wang, Y.X. Wei, Y.X. Hou, H.P. Shuai, J.P. Cai, J.F.W. Chan, J. Zhou, K.Y. Yuen, Human coronavirus dependency on host heat shock protein 90 reveals an antiviral target, Emerg. Microb. Infect. 9 (2020) 2663–2672.
[42] Y.X. Liao, Y.L. Ye, S.M. Li, Y.L. Zhuang, L.Y. Chen, J.X. Chen, Z.N. Cui, L.J. Huo, S.W. Liu, G.P. Song, Synthesis and SARs of dopamine derivatives as potential inhibitors of influenza virus PA_N endonuclease, Eur. J. Med. Chem. 189 (2020) 112048.